EARTHQUAKE SOURCE PARAMETERS, SEISMICITY, AND TECTONICS OF THE OCEANOGRAPHER TRANSFORM FAULT

by

JAMES LOUIS MULLER

B.S., Virginia Polytechnic Institute and State University
(1971)

SUBMITTED TO THE DEPARTMENT OF
EARTH AND PLANETARY SCIENCES
IN PARTIAL FULFILLMENT OF THE
REQUIREMENTS FOR THE DEGREE OF

MASTER OF SCIENCE IN GEOPHYSICS

at the

MASSACHUSETTS INSTITUTE OF TECHNOLOGY

May, 1982

Signature of Author . . . . . .
Department of Earth and
Planetary Sciences

Certified by . . . . . .
Sean C. Solomon
Thesis Supervisor

Accepted by . . . . . .
Theodore R. Madden
Chairman, Department
Graduate Committee

ABSTRACT

EARTHQUAKE SOURCE PARAMETERS, SEISMICITY, AND TECTONICS OF THE OCEANOGRAPHER TRANSFORM FAULT

by

JAMES LOUIS MULLER

Submitted to the
Department of Earth and Planetary Sciences
on May 24, 1982
in partial fulfillment of the requirements for the
degree of Master of Science

Earthquakes on oceanic transform faults provide a record of plate motion in space and time. This thesis is a study of the recent history of displacement on the Oceanographer transform fault as revealed by the source characteristics of teleseismically recorded earthquakes. The largest known earthquake on the transform is the M_S = 6.3 event of May 17, 1964. Synthesis of the P waveforms from this event indicates a strike-slip mechanism on a nearly vertical fault oriented along the transform, with a seismic moment of 9.9×10^{25} dyne-cm. The focal depth is 4 ± 1 km below the sea floor. The preferred source mechanism involves rupture propagation from east to west on a fault 12 km long, and an average displacement of about 5 m. The total seismic moment released by earthquakes since 1920 is estimated and agrees with the cumulative moment predicted by the transform length and the local spreading rate if the average fault width is about 5 km. The historical record of large earthquakes on the Oceanographer transform indicates that the transform slips in a jerky manner and along small segments rather than in large events involving rupture along the entire length of the transform. The repeat time for $M_S \simeq 6$ events on that part of the transform fractured by the May 17, 1964 event is about 200 yrs, and the recurrence interval on the entire transform for earthquakes similar to the 1964 event is 15-20 yrs.

Thesis Supervisor: Sean C. Solomon
Associate Professor of Geophysics

TABLE OF CONTENTS

ACKNOWLEDGEMENTS

This research was partially supported by the National Science Foundation, Earth Sciences Section, under NSF Grants EAR 77-09965 and EAR-8115908.

CHAPTER 1. INTRODUCTION

GENERAL CONCEPT OF TRANSFORM FAULTS

Oceanic transforms are lateral offsets of oceanic ridges, representing a discontinuity along the ridge length of the emplacement of crustal material beneath the ocean floor. They are recognizable by lateral offsets in the seismicity and topographic expression of the adjoining ridge segments, and by fracture zones, linear topographic and magnetic features extending away from, and at right angles to, the ridge segments. The existence of fracture zones has been known for some time, but until 1965 they were regarded as transcurrent faults along which the adjoining ridge segments were moving away from each other. According to this interpretation earthquake activity should be distributed along the entire fracture zone, and the slip direction should carry the ridge segments away from each other, i.e., if the ridge were offset to the right, then the direction of earthquake motion should be right-lateral strike-slip.

Wilson (1965) noted that, according to sea-floor spreading theory, oceanic ridges represent zones along which plates of the earth's lithosphere move apart from each other. He therefore proposed that the offsets of ridge axes are zones of shear between plates moving away from the adjoining ridge segments. Wilson (1965) called this new interpretation of the ridge offsets "transform faults". According to this interpretation, the direction of slip during earthquakes on these faults should be in the opposite direction to that of the ridge offset, the seismicity along these faults should be limited to the "active" section between the adjoining ridge segments, and the long topographic

and magnetic features which extend away from the ridge segments are simply scars on the ocean floor produced when that crust had been part of the active transform. By relocating and preparing fault plane solutions for many ocean floor earthquakes, Sykes (1967) showed that most ocean floor seismic activity was indeed limited to the "active" portion of transform faults and that the direction of fault slip was opposite to that of the ridge offsets, thus confirming Wilson's (1965) interpretation. Transforms are steady-state features of constant length, which terminate sections of active emplacement of material onto the oceanic lithosphere and crust, and at which parts of the ocean floor with different age are in contact. In this thesis we take a closer look at the seismicity and source parameters of major earthquakes on an oceanic transform fault in order to characterize the motion on the transform in space and time.

GEOLOGIC SETTING OF NORTH ATLANTIC TRANSFORM FAULTS

In the central and north Atlantic Ocean, transform faults along the Mid-Atlantic Ridge range in length from less than a few tens to several hundred kilometers. Common bathymetric features reported for transform faults include a deep central trough which, at its deepest point, can be as much as a thousand meters deeper than the surrounding sea floor. Another feature found sometimes on one side, and sometimes on both sides, of the transform is an elevated "transverse" ridge, running parallel to the transform valley and forming walls which can be as much as a thousand meters higher than the surrounding sea floor and 10 km wide (e.g., van Andel et al., 1971; Fleming et al., 1970; Detrick and Purdy, 1980). The troughs typically obtain their greatest depths in depressions located at the intersections of the transform and the adjacent ridge segments.

The topographic expressions are present not only on the active portion of each transform, but extend several thousand kilometers away from the ridge into older ocean floor. The topographic features are accompanied by magnetic and gravitational anomalies.

Small-scale topographic features have been studied for a few of the transforms on the Mid-Atlantic Ridge. Detrick et al. (1973) and ARCYANA (1975) report that the inner walls of the transverse ridges flanking the active fault section of Fracture Zone A, a small transform near 37° N, have scarps ranging in size from 10 cm to several tens of meters. Similar structures were reported by Oceanographer Transform Tectonic Research Team (1980 a,b) from work of ALVIN and ANGUS on the Oceanographer transform. Schroeder (1977) reports that the inner walls of the Oceanographer transform are made up of steep, sediment-covered scarps, 100 to 1000 m high. At least for these two transforms the inner walls seem to be made up of faulted blocks of material, whose faces have considerably greater slopes than the average slope of the inner walls. Eittreim and Ewing (1975) presented results from a seismic reflection survey of the Vema transform fault, which showed that the entire valley floor was covered with thick sediment and that this sediment was cut by a fault-like feature for the entire length of the transform. The implication was that this feature is a zone along which recent strike-slip motion has taken place.

Results have been published from three seismic refraction experiments designed to measure the crustal structure beneath fracture zones. Two of these (Fox et al., 1976; Detrick and Purdy, 1980) were on non-active limbs of fracture zones. Fox et al. (1976) found that the basement crustal structure of the western limb of the Oceanographer Fracture Zone consisted of an upper layer with a compressional velocity

of 4.4 km/sec and a thickness of 2.1 km, and a second layer with a velocity of 6.5 km/sec. They did not observe any mantle arrivals, and thus were able only to estimate the minimum thickness of the second layer by assuming various velocities for the mantle. For assumed mantle compressional velocities of 7.0, 7.5, and 8.2 km/sec they obtained a minimum thickness for the second layer of 2.5, 3, and 4 km, respectively. Detrick and Purdy (1980) reported the results of a detailed refraction study of the eastern non-active limb of the Kane Fracture Zone. Their results showed the crust there to consist of only one layer over the mantle. The layer had a compressional velocity of 4 to 5 km/sec and a thickness of 2 to 3 km. The mantle had a compressional velocity of 7.7 to 8.0 km/sec. This result has both crustal thickness and average crustal velocities considerably lower than those of normal ocean crust. Ludwig and Rabinowitz (1980) reported results from a seismic refraction and reflection experiment in the active section of the Vema transform fault. Their results showed the transform valley to be filled with about 1500 m of sediment, and the depth to the basement ranged from 6200 to 6700 m. Below this depth they found a two-layer crust, with the first layer having a compressional velocity of 4.3 km/sec and a thickness of 2 km, and the second layer having a compressional velocity of 5.9 to 6.2 km/sec and a thickness of 2.6 km. They reported that the structure had significant variation and that it was impossible to identify any consistent layer with those of a normal ocean floor.

Solomon (1973) examined the attenuation of shear waves from a large earthquake on the Gibbs transform and found greater attenuation for stations for which the ray paths passed under the western intersection of the transform and the adjoining ridge segment than for stations whose ray

paths went elsewhere. The implication was that a zone of low Q material existed beneath the western end of the Gibbs transform, possibly indicating a hotspot or zone of partial melting. Rowlett and Forsyth (1979) reported abnormally high residuals for the P-wave travel times from a distant earthquake as observed by an array of ocean-bottom seismometers at the western end of the Vema transform fault. The size and distribution of the residuals implied that under part of the intersection of the transform and the adjoining ridge segment there must exist a zone with lower than normal seismic velocities which extends quite far into the mantle. They suggested that this might be a magma chamber or a zone of partial melting. This interpretation is similar to that of Solomon (1973).

TRANSFORM FAULT SEISMICITY

Earthquakes on oceanic transform faults have been shown to be strike-slip and in a direction consistent with Wilson's (1965) hypothesis of transform faults (e.g., Sykes, 1967, 1970). Isacks, Oliver, and Sykes (1968) showed that the maximum sizes of earthquakes observed on transform faults were larger than those on oceanic ridge crests, but smaller than those on island arc-subduction zone systems, probably reflecting the relative amount of lithosphere in contact at each of these boundaries. Sykes (1967) showed that transform fault earthquakes are primarily confined to the active transform section between the adjoining ridge segments. This finding has been verified by several experiments using arrays of ocean-bottom seismometers (e.g., Rowlett, 1981; Project ROSE Scientists, 1981).

Transform fault earthquakes generally occur at shallow depths. Weidner and Aki (1973) studied the surface waves from event pairs on the

Mid-Atlantic Ridge, and found the focal depths of two strike-slip events to be 6 ± 3 km below sea floor. Project ROSE Scientists (1981), using a large array of ocean-bottom seismometers, found that the microearthquakes on the Orozco transform were limited to depths shallower than 17 km.

Teleseismically determined epicenters of transform earthquakes are generally scattered over a zone that is as wide as 30 km. This may be due to poor epicentral determinations or it may indicate that seismic activity is distributed over a broad area. Epicenters determined by Project ROSE Scientists (1981) for the Orozco transform were divided into two groups. One group, near the western end of the transform, showed clear alignment along a narrow trough parallel to the slip direction between the Cocos and Pacific plates, and the first motions of these events were consistent with strike-slip faulting along the transform. The other group occurred near the center of the transform, in a topographically complicated region, and did not show any preferred alignment with the strike of the transform. One interpretation is that the microseismicity is composed of both strike-slip activity and other activity, possibly related to topographic features. This would be consistent with the interpretation of Eittreim and Ewing (1975) that the linear feature they observed in the sediments of the Vema transform represented a narrow zone of stike-slip motion. Microearthquakes at the ends of transforms on slow spreading ridges do not exhibit alignment with the transform strike, but instead are generally scattered about the inner walls of the depressions usually observed at transform ends (e.g., Rowlett, 1981), which suggests that these events are related to processes unique to transform-ridge intersections.

There is evidence that the size of transform fault earthquakes is

related to the dimensions and slip rate of the transform. Burr and Solomon (1978) found that (1) the maximum seismic moment decreases with slip rate and increases with transform length up to lengths of about 400 km, (2) average fault width increases with transform length and decreases with slip rate, and (3) larger earthquakes generally occur toward the center of a transform. They interpreted these results as indicating that the lower boundary of seismic activity is defined by an isotherm, conservatively determined to be between 50°C and 300°C. This is consistent with the finding of shallow focal depths for transform earthquakes.

LARGE EARTHQUAKES ON NORTH ATLANTIC TRANSFORMS

Weidner and Aki (1973) studied two strike-slip earthquakes from the North Atlantic Ocean which occurred on May 17, 1964 and June 9, 1970. Epicenters of these events were 35.29° N, 36.07° W, and 15.4° N, 45.9° W, respectively. Both of these events had m_b = 5.6. Weidner and Aki (1973) found seismic moment values for these events of 1.03×10^{25} dyne-cm and 1.94×10^{25} dyne-cm, respectively.

Kanamori and Stewart (1976) performed a detailed study of the surface waves and body waves from two earthquakes on the Gibbs transform which occurred on Feb. 13, 1967 and Oct. 16, 1974. They found seismic moments for these events of 3.4×10^{26} dyne-cm and 4.5×10^{26} dyne-cm, respectively. By assuming bilateral rupture propagation, they found fault lengths of 60 km and 72 km. With these values and assuming a fault width of 10 km, they found displacements of 160 cm and 180 cm and dislocation velocities of 23 cm/sec and 18 cm/sec, respectively. An important implication was that these events exhibited slower than normal fault movement and therefore excited much greater long-period surface

waves than usual for events of this m_b. By comparing the displacements and fault lengths of these events to the total length of the transform and the rate of slippage predicted by magnetic anomalies, and by assuming that previous large earthquakes on the transform were similar to these, they concluded that the Gibbs transform slips in a jerky manner, with major events alternating between the eastern and western half. The time for one complete cycle is about 26 years, with the entire transform slipping once during this period.

OBJECTIVES OF THIS STUDY

Previous work on transform fault earthquakes has shown them to be strike-slip, reflecting the relative motion of plates across the transform. It has also shown them to be shallow, and in some cases, limited to a narrow zone of seismic activity. Burr and Solomon (1978) showed that there is some connection between a transform fault's dimensions and slip rate and the earthquakes which occur on the transform. From the study of Kanamori and Stewart (1976), the earthquakes gave us some clues as to how the Gibbs transform behaves, although the earthquakes themselves seemed to be somewhat unusual.

In this work we examine the seismicity and largest earthquake of the Oceanographer transform. Our goal is to try to understand the motion of this transform, and in particular to focus on the following questions: What are the main source parameters of the large earthquake which occurred on 17 May 1964? How deep in the crust or mantle did it occur? Was this earthquake similar to those on the Gibbs transform studied by Kanamori and Stewart (1976)? Did it exhibit abnormally high or low stress-drop or displacement? Does this transform slip smoothly or does it move in discrete, jerky episodes? What is the repeat time for

seismic episodes on any section of the transform? Has the entire transform slipped at least once during its known seismic history? Is the seismicity restricted to one narrow zone of slippage or is it as widely scattered as the teleseismically-determined epicenters indicate? Does the background seismicity represent the same kind of motion as the larger events?

To try to answer these questions we have constructed synthetic seismograms for comparison to the observed P waveforms from the large earthquake of May 17, 1964. The technique adopted for P-wave synthesis is described in Chapter 2. On the basis of the P-wave modeling we have determined source parameters for the 1964 event. We have also combined data from the known seismicity of the transform with the parameters found for this large earthquake to estimate the observed seismic slip rate, for comparison to the rate of slip predicted from magnetic anomalies. The results are presented in Chapter 3 of this work. Finally, in Chapter 4, we describe plans for extending the study presented in this thesis to other transform faults in the north Atlantic.

CHAPTER 2. METHOD OF P-WAVE SYNTHESIS

We have constructed synthetic seismograms of the P-waves for comparison with the observed seismograms from the largest strike-slip earthquake on the Oceanographer transform fault. By matching the synthetic waveforms and amplitudes to observed ones we have been able to determine some of the source parameters and other features of the event.

We have used the method of Langston and Helmberger (1975), used also by Kanamori and Stewart (1976) and Chung and Kanamori (1976), with some modifications of our own. The basic approach is a time-domain superposition of the direct P, pP, and sP phases. The pP and sP phases are delayed by an amount appropriate to the event depth and adjusted in amplitude by the reflection coefficient for the top of the oceanic crust. The amplitude of each phase is corrected for the radiation pattern of the event, and the final time series is corrected for geometric spreading, attenuation, instrument response, and the effect of the free surface near the receiver.

According to Love (1934), the far-field displacement for a double-couple point source in a uniform, unattenuating medium can be expressed by

$$u_p(t) = \frac{1}{4\pi\rho v^3} \dot{M}(t-r/v) \; R_{\theta,\phi} \qquad (2.1)$$

where r is the distance, ρ is the density, v is the wave velocity, $R_{\theta,\phi}$ is a factor for the radiation pattern, $\dot{M}$ is the time derivative of the seismic moment, and t is time. We can think of $\dot{M}$ as the rate of generation of seismic moment. If we express $\dot{M}$ as

$$\dot{M} = M_0 \, T(t) \qquad (2.2)$$

where M_0 is the scalar seismic moment and $T(t)$ is a time series such that

$$\int T(t)\, dt = 1, \tag{2.3}$$

then $T(t)$ represents a normalized displacement function with the same shape as would be observed as a direct P wave at teleseismic distances. The far field displacement expression (2.1) then becomes

$$u_p(t) = \frac{1}{4\pi\rho v^3} M_0 R_{\theta,\phi} T(t-r/v). \tag{2.4}$$

P-wave arrivals on observed seismograms are composed principally of the direct P and the surface reflections pP and sP. We can express these reflected phases by using the appropriate radiation pattern factor $R_{\theta,\phi}$, multiplying by the free surface reflection coefficient $A(i_r)$, where i_r refers to the emergent angle at the piont of reflection for the phase i, and then delaying each phase Δt for the extra travel path length due to the event depth. The complete waveform is then the sum of these phases and can be expressed as

$$u(t) = \frac{1}{4\pi\rho v^3} M_0 \left(T(t-r/v)\, R_1 + T(t-r/v-\Delta t_2)\, R_2\, A_2 + T(t-r/v-\Delta t_3)\, R_3\, A_3\right) \tag{2.5}$$

where the subscripts 1, 2, and 3 refer respectively to the P, pP, and sP phases.

To obtain the final synthetic seismogram we correct this expression for geometric spreading, attenuation, crustal effects at the receiver, and instrument response. The result can be expressed as

$$u_{syn}(t) = u(t)\ \frac{g(\Delta,h)}{a}\ C(i_0)\ *\ \frac{F(t/t^*)}{t^*}\ *\ I(t) \tag{2.6}$$

where a is the radius of the earth, $g(\Delta,h)$ is the geometric spreading factor, $C(i_0)$ is the free surface effect at the receiver, i_0 is the incident angle at the receiver, $F(t/t^*)$ is the attenuation operator, $I(t)$

is the instrument response, * means the convolution operation, Δ is the epicentral distance to the station, h is the focal depth, and t^* is the attenuation parameter defined as the ratio of travel time to the average quality factor Q along the ray path.

Several of the factors in the above expressions have been given in previous work. The radiation pattern factors (R_i's) have been given by Kanamori and Stewart (1976). The free surface correction $C(i_o)$ is given in Bullen (1965). The geometric spreading factor $g(\Delta,h)$ is given by Kanamori and Stewart (1976) as

$$g(\Delta,h) = \left(\frac{\rho_h \beta_h}{\rho_o \beta_o} \frac{\sin i_h}{\sin \Delta \cos i_o} \left| \frac{di_h}{d\Delta} \right| \right)^{1/2} \qquad (2.7)$$

where the subscripts h and o refer to the source and receiver respectively. The incident angles for this expression were calculated using travel times from Herrin (1968) and the velocity appropriate to the depth for the source structure, and using a velocity of 6.0 km/sec for the receiver. The attenuation function $F(t/t^*)$ corresponds to a linear, causal, constant-Q, slightly dispersive earth model calculated by Carpenter (1966) from the work of Futterman (1962) and Kolsky (1956). [The paper of Carpenter (1966) has been reprinted by Toksoz and Johnston (1981).] The instrument response correction I(t) is taken from the frequency domain correction given by Hagiwara (1958). The reflection coefficients A_i are given in Ewing et al. (1957), though for potential amplitude rather than displacement amplitude. This makes no difference for the pP conversion. For the sP conversion however it means that we must also use the additional factor of

$$B_{sP} = \frac{\beta}{\alpha \sqrt{3}} \frac{\cos i_p}{\cos i_s} \qquad (2.8)$$

where α is the P-wave velocity and β the S-wave velocity where the reflection takes place, i_s is the S-wave incident angle on the surface, and i_p is the emergent angle of the reflected P-wave. Thus the sP term in (2.5) becomes $T(t-r/v-\Delta t_2)\ R_2\ A_2\ B_{sP}$. For all of these calculations and for the velocity models used we have assumed a Poisson solid, i.e., $(\alpha/\beta)^2 = 3$.

We have made two improvements to the previously used versions of this method for P-wave synthesis. The first is the use of a layered velocity structure near the source. In previous applications of this technique (e.g., Kanamori and Stewart, 1976) the structure near the source was assumed to be a simple half-space. In order to improve the accuracy of the depth dependence of the results we used a layered structure, in which the actual properties of the faulted material depend on the layer in which the event occurred. The calculation of the delays Δt_i for the pP and sP phases were made by tracing the reflected P from the depth of the event up to the surface and then, as the original s or p phase, back down to the event, changing the emergent angle at each interface encountered. The final delay value was a summation over the j layers of a path-length component and a horizontal component,

$$\Delta t = \sum_j h_j \left(1/(v_j \cos i_j) - (\tan i_j)/p\right) \qquad (2.9)$$

where h_j is the thickness of layer j, i_j is the emergent angle in layer j, v_j is the wave velocity in layer j, and p is the horizontal phase velocity for that epicentral distance and event depth. This summation over the j layers is done twice, once for the reflected P, from the event depth up to the surface, and once back down to the event for the original p or s phase, using the velocities and emergent angles appropriate for

that phase. Figure 2.1 illustrates how these corrections were determined.

The other modification we have introduced is the use of a finite fault, and the resulting variation of the apparent source time function T(t) with emergent angle and station azimuth. We assume that faulting begins at the event focus and propagates for some finite length with a constant propagation velocity. We allow the fault to be either unilateral or bilateral, and in the latter case we assume that the two arms of the fault are of equal length. We assume that propagation occurs horizontally along the strike of the fault. We can then calculate the angle Q between the propagation vector and the ray to any station i by

$$\cos Q_i = \cos\theta \cos d_i + \sin\theta \sin d_i \cos\phi \cos Az_i + \sin\theta \sin d_i \sin Az_i \sin\phi, \tag{2.10}$$

where Az_i and d_i are the azimuth measured clockwise from north and emergent angle measured up from vertical, respectively, for the ray to station i, ϕ is the azimuth of the propagation vector, measured clockwise from north, and θ is the angle of the propagation vector measured from vertical. This geometry is illustrated in Figure 2.2. For horizontal propagation, we have $\theta = \pi/2$, so that equation (2.10) reduces to $\cos Q_i = \sin d_i \cos(\phi - Az_i)$. (In Figure 2.2 we also show the fault dip δ. The fault dip is used in determining the effect of finite fault width on the source time function.)

The apparent propagation time T_i, as seen at station i, for any unilateral event with fault length L and propagation velocity v_{pro} will be

$$T_i = L\,(1/v_{pro} - (\cos Q_i)/v). \tag{2.11}$$

As shown in Figure 2.3, this represents the propagation time plus (or minus, depending on the propagation direction) a correction for the extra

path length required by source finiteness. For a bilateral fault the result will simply be the superposition of two simultaneous equal-length unilateral faults propagating in opposite directions. The time function corresponding to this apparent propagation time is then convolved with two other time domain functions, one representing the rise time of the displacement, and the other representing nearly instantaneous rupture along the fault width. The rise time function is taken as a rectangular boxcar function, with a duration equal to the rise time. The fault width function is calculated in the same manner as the propagation time function T_i, except that v_{pro} is assumed to be infinite in (2.11), and Q_i is taken from (2.10) with $\pi/2-\delta$ replacing θ. Thus the apparant source time function, and therefore the waveform, of the synthetic seismogram for each station varies with the emergent angle and azimuth of the ray to that station. This effect can be important for horizontally propagating faults (including large transform fault events), particularly for unilateral rupture.

The last correction mentioned above assumes nearly infinite propagation of the rupture along one dimension of the fault, so that the other dimension, which shows a finite propagation time, represents linear propagation of a line source. We realize that this is not a physically reasonable model for actual rupture propagation. We believe that this objection is not significant, however, because there is not enough precision available in the shape of observed P-waves to justify the use of a more complicated model. There is one significant objection that can be raised, however, which involves the calculation of the pP and sP delay times for a horizontally propagating fault. If the fault plane is nearly vertical, such as for a strike-slip fault, and if the fault propagates

horizontally, then the initiation of rupture is assumed to take place simultaneously along a vertical line. This means that the up-going pP and sP waves begin at a different depth from the down-going direct P. If for example the fault has a width of 4 km and extends from the surface down to 4 km, then the pP and sP phases would arrive at a receiver simultaneously but behind the direct P phase by the time required to travel vertically the extra 4 km. Such a situation is not likely because the initiation of rupture is more likely to occur at a point than along a line, and this point can be located anywhere along the fault's width. We therefore assume that the focal depth is a point source rather than a line source for the purposes of calculating the pP and sP delay times. This means that we should use, for our "fault width" convolution of the source time function, some non-rectangular function which represents the build-up of rupture away from the point of origin into the line source which will ultimately propagate horizontally. This would mean, as above, the inclusion of a correction for wave shape which cannot be resolved from the shapes of observed P-waves. Therefore we have not included this additional complexity, even though we realize it introduces an incompatibility between two facets of our model.

As a check of our method, we computed synthetic seismograms of P waves and compared them to the results of Langston and Helmberger (1975). For this comparison we used their source velocity structure, which consisted of a halfspace with a seismic velocity of 6.0 km/sec and a density of 2.7 g/cm^3. We computed seismograms for a strike-slip earthquake, as observed at a station with an epicentral distance of 80° and on an azimuth 45° from the strike of the fault. We used two sets of source dimensions and rise times, which produced the source time

functions given by Langston and Helmberger (1975) as representing a low stress-drop earthquake and a high stress-drop earthquake. This was a trapezoidal time function, with a rising ramp of 0.5 sec duration, a plateau of 1.5 sec duration, and a falling ramp of 0.5 sec duration for the high stress-drop case, and values of 2.0 sec, 6.0 sec, and 2.0 sec, respectively, for these variables in the low stress-drop case. Synthetic seismograms were computed for focal depths of 5, 10, 15, and 20 km. The resulting waveforms are shown in Figure 2.4 and are practically identical to the waveforms given in Figure 4 of Langston and Helmberger (1975).

Other methods of constructing synthetic seismograms have been constructed which involve superposition of eigenfunctions in wave number space, e.g. Bouchon and Aki (1977). Our method offers the advantage that it is numerically simpler and requires less computer time. Because our method is a time domain synthesis, it is easier to understand the contribution to the result from each of the fault parameters, and to adjust these parameters to bring about the desired result. The major difference in the techniques as applied to a layered structure for a transform fault is the presence of water reflections in the normal mode superposition which are not included in our results. These reflections do not influence the first 10 seconds of so of each seismogram, the part most critical to our analysis.

The primary limitation to our method is that we do not include any phases or reflections other than P, pP, and sP. For most earthquakes there are complexities in the signal introduced by the layered velocity structure near the source; reflections and phase conversions at the interfaces can introduce other phases into the final waveform. For

oceanic earthquakes there is also a large contribution from surface reflections of the upgoing p wave in the water. We generally do not try to fit observed waveforms after the first 10 sec or so because we have not included these phases. The reflections and phase conversions at the interfaces in the oceanic crust do not contribute much to observed waveforms, because the amplitudes are too small. Figure 3-16 in Ewing, Jardetsky, and Press (1957) shows that, for a typical interface in an oceanic crust, the amplitude ratios of reflected or transmitted P waves from incident SV waves are only about .05 to .07 for the range of emergent angles used here. Figure 3-15 in Ewing, Jardetsky, and Press (1957) shows that for these interfaces and emergent angles the amplitude ratio of reflected P waves to incident P waves is less than .05. One other factor influencing any internal reflections in the layers of an oceanic crust is that the Q values for these layers may be fairly low; any internal reflections must pass through these layers several times and thus would have amplitudes even further reduced compared to the P, pP, and sP phases. These phase conversions and reflections could be included in our method, but it would contribute to the computational complexity which we have tried to minimize.

Another source of waveform complexity is the contribution introduced by a layered velocity structure beneath each receiver. We did not try to correct for this because each receiver would have its own structure.

With our method the following independent variables must be given: P-wave velocity and density for each layer in the structure near the source, station azimuths and distances, event depth, fault strike and dip, slip angle, fault length and width, rupture propagation velocity, rise time, propagation direction information (bilateral or unilateral

and, if unilateral, which direction), attenuation value t^*, and total scalar moment. Of these, all but the velocity and density structure and station azimuths and distances are unconstrained by other considerations and therefore are, in principle, resolvable within the limits of the available observed seismograms.

The observed seismograms used for comparisons to the synthetic seismograms were taken from the long-period vertical records of WWSSN stations, generally in Europe and North America and around the North Atlantic Ocean. The records were digitized at an interval of 0.6 sec and plotted, along with the synthetic seismograms, with normalized amplitudes to facilitate waveform comparison. Total moment was determined by numerically matching the maximum amplitude, taking into account which part of the waveform was being compared. Other parameters were determined by visual comparison. The epicenters used for determining distances and azimuths were taken from the Bulletins of the International Seismological Centre, and the travel times and ray parameters were calculated from the tables of Herrin (1968).

Figure Captions

Figure 2.1 Contributions to the delay times of pP and sP phases with respect to the direct P phase. The contribution from each leg of the wave path is determined by dividing the path length by the appropriate seismic velocity. An additional correction to the teleseismic travel time is determined from the phase velocity and the total horizontal separation between source and reflection path at the focal depth.

Figure 2.2 Geometry used in determining the angle Q_i between rupture propagation vector and the ray path to station i. ϕ is the strike of the fault plane, measured clockwise from N. For horizontal propagation, ϕ is also the azimuth of the propagation vector. δ is the dip of the fault plane, measured from the horizontal.

Figure 2.3 Total apparent propagation time is composed of a term for the actual time of rupture propagation and a term proportional to the difference L cos Q_i in path lengths from each end of the fault to station i.

Figure 2.4 Synthetic seismograms determined for a strike-slip earthquake, for the high stress-drop and low stress-drop cases of Langston and Helmberger (1975) for focal depths of 5, 10, 15, and 20 km. These waveforms are comparable to those in Figure 4 of Langston and Helmberger (1975).

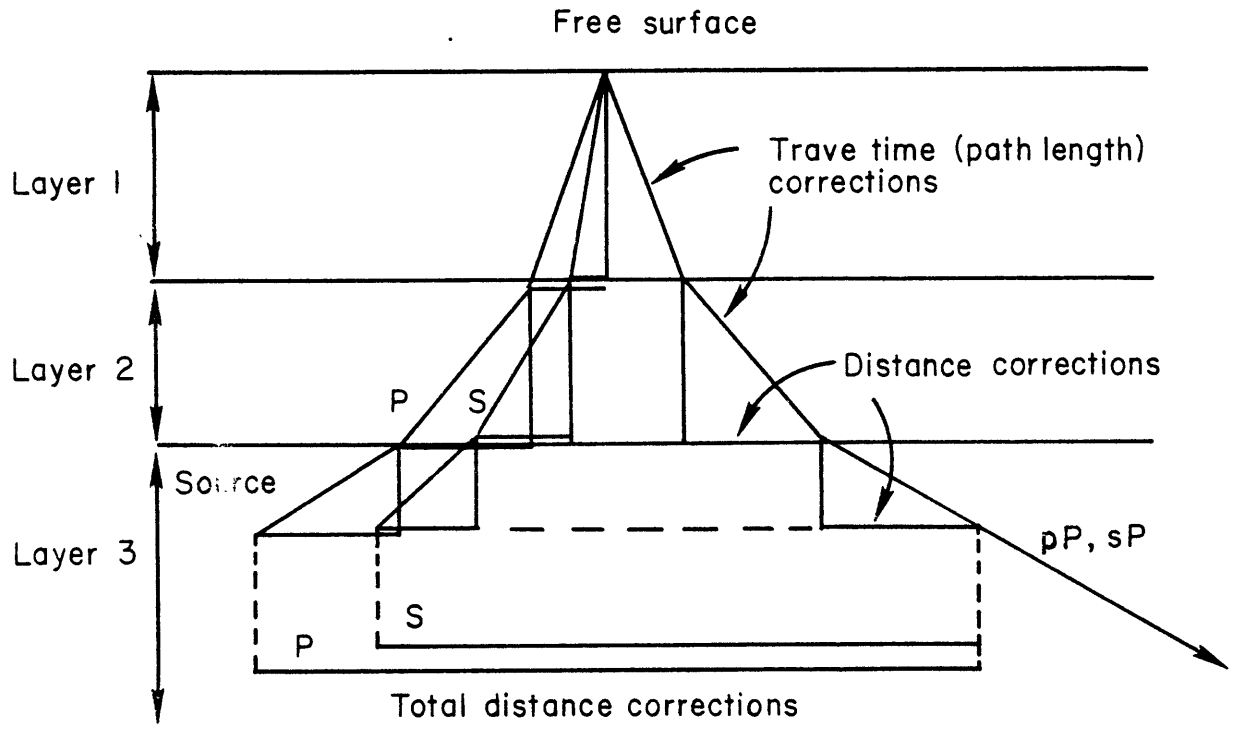
Free surface
Layer 1
Layer 2
Layer 3
Trave time (path length) corrections
Distance corrections
P
S
Source
pP, sP
S
P
Total distance corrections

Figure 2.1

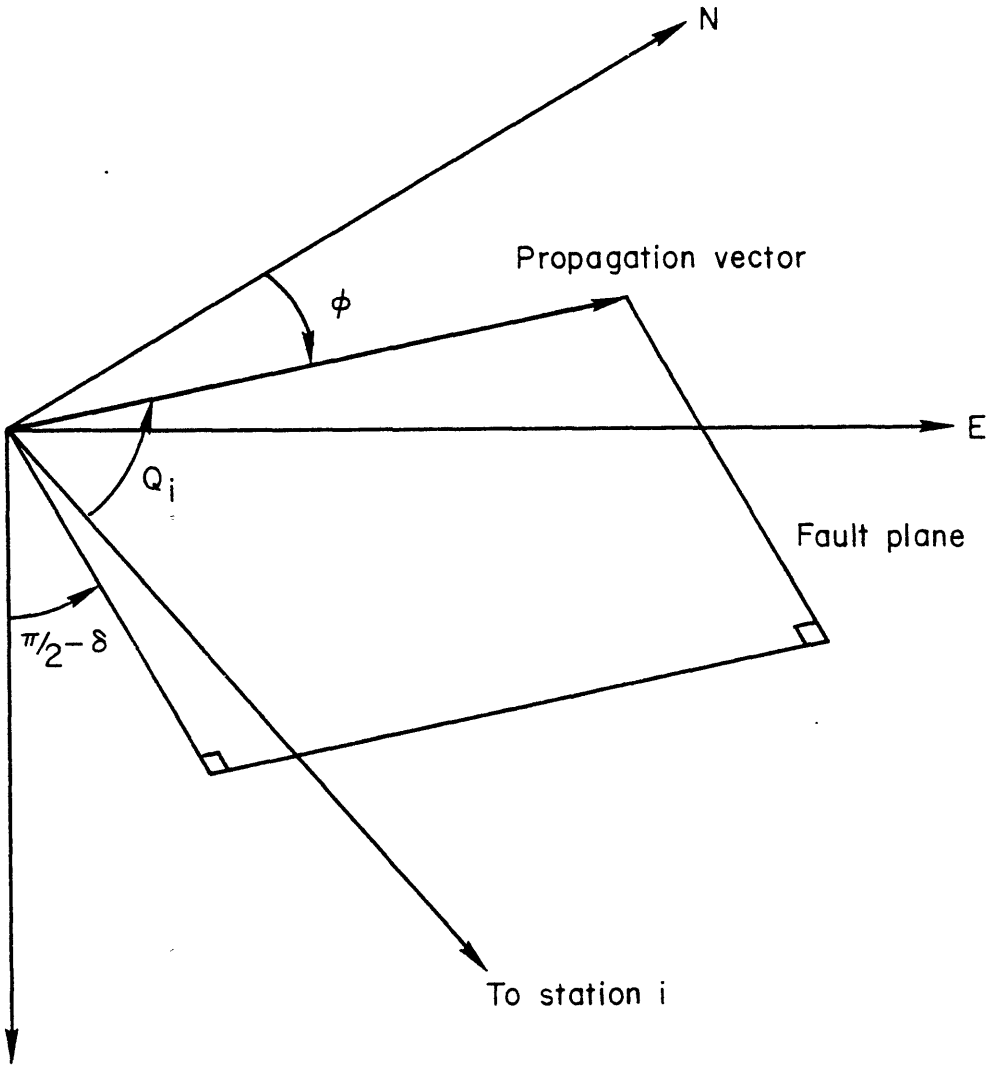
N
Propagation vector
ϕ
E
Q_i
Fault plane
$\pi/2-\delta$
To station i

Figure 2.2

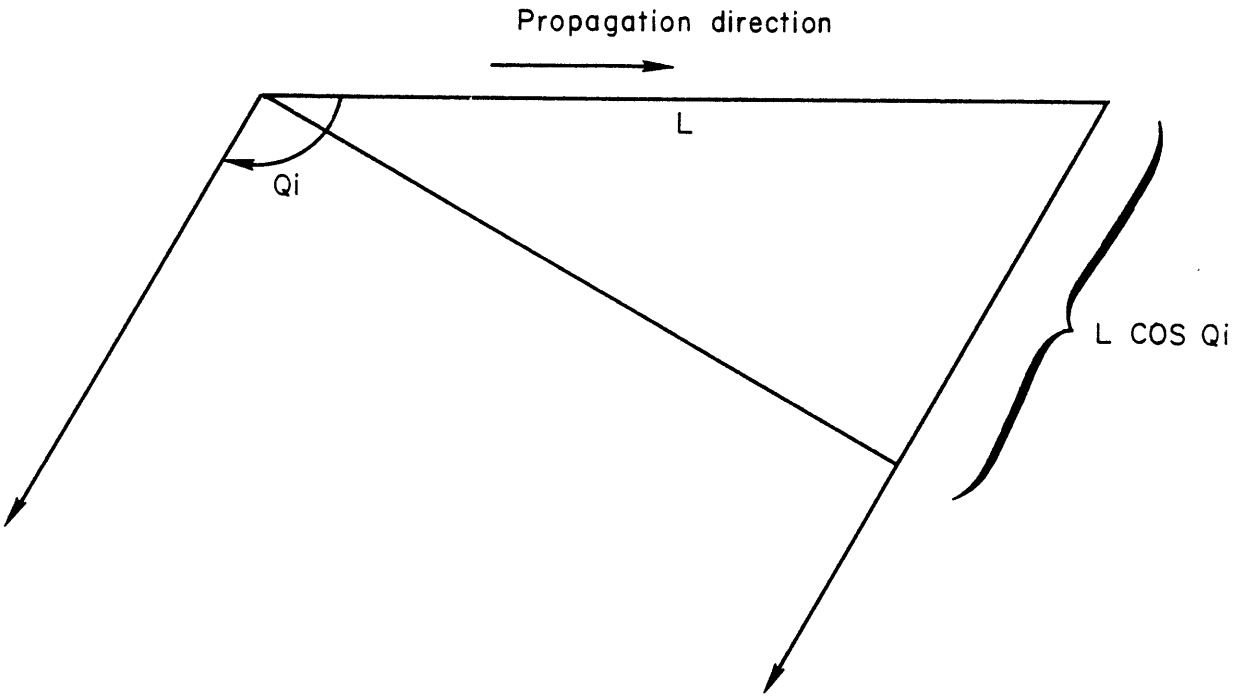

Figure 2.3

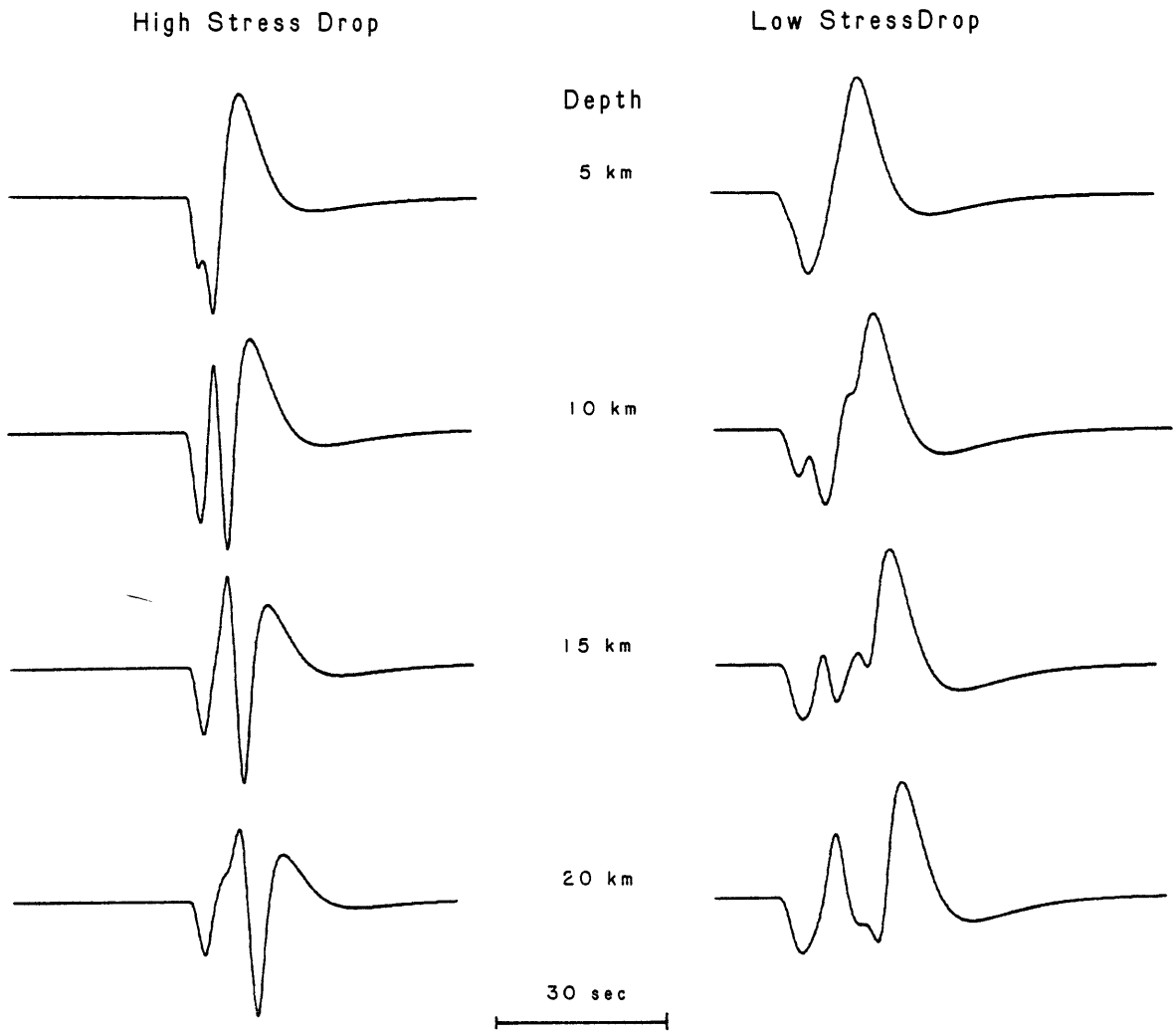
High Stress Drop
Low StressDrop
Depth
5 km
10 km
15 km
20 km
30 sec

Figure 2.4

CHAPTER 3. EARTHQUAKES AND TECTONICS OF THE OCEANOGRAPHER TRANSFORM FAULT

In this chapter we review the known features of the Oceanographer transform fault and then present the results of our study of the earthquakes of the area. The study includes a survey of the seismicity, P-wave synthesis for the largest known earthquake on the transform, and analysis of the behavior of the transform as a plate boundary.

The Oceanographer Fracture Zone offsets the Mid-Atlantic Ridge right-laterally by about 130 km near 35°N. Its existence as an east-west trending section of the Mid-Atlantic Ridge was first noted by Heezen et al. (1959). Sykes (1967) analyzed the first motion polarities of P waves from an earthquake which occurred on May 17, 1964 on the transform portion of the Oceanographer Fracture Zone. He showed that the motion was left-lateral strike slip on a nearly vertical fault and was therefore compatible with Wilson's (1965) concept of a transform fault. The area was surveyed in 1967 by the USCGS Oceanographer and in 1973 and 1974 by the R/V Vema. The results of the surveys were presented by Fox et al. (1969,1976) and by Schroeder (1977). The transform was also the subject of investigation by ALVIN and ANGUS, the results of which were presented by the Oceanographer Transform Tectonic Research Team (1980 a,b).

The bathymetry of the Oceanographer transform fault, shown in Figure 3.1, is characterized by a v-shaped valley which runs down the center of the transform, i.e., on a strike of roughly 105° from north, and by ridges which run parallel to and on each side of the the valley. The width of the valley below the 3000 m contour varies between 8 and 35 km.

The maximum depth of the central valley varies along its length between 3600 m and 4800 m below sea level, reaching a maximum depth in a depression near the eastern end where the transform intersects the adjoining ridge segment. A corresponding depression exists at the western end, which Schroeder (1977) reports as having a depth to the basement of at least 4000 m below sea level and a covering of roughly 250 m of sediment. Similar depressions have been reported at the ends of other transform faults in the North Atlantic, e.g., the Gibbs and Kane transform faults, and are believed to be caused by the loss of hydrostatic pressure due to the viscosity of the upward moving mantle material (Sleep and Biehler, 1970). The ridges which flank the transform valley rise to depths shallower than 2000 m below sea level, with the southern ridge higher in the west and the northern ridge higher in the east. Schroeder (1977) reports that the slope of the walls between the ridges and the central valley varies between 10° and 24°, with an average of 16° for the southern wall and 12° for the northern wall; he reports that when the effects of sediment are removed from the bathymetric data, the walls appear to be made up of scarps which vary in height from 100 to 1000 m, and have slopes which generally fall between 20° and 40° but can be as high as 60°. Schroeder (1977) suggests that these scarps are actually fault envelopes containing numerous fault planes which may dip very steeply; this inference is made from personal communication from P.J. Fox on dredge haul results, and from direct observations of similar fault envelopes in the FAMOUS area (ARCYANA, 1975). The southern wall is dominated by a peak at its western end, near where the transform ridge merges with the eastern flank of the adjoining spreading center. This peak creates an apparent bend in the bathymetric trend of the transform

valley and may be related to a source of seismic stress concentration at this point. A similar peak exists at the eastern end of the northern wall, though the trend of the transform valley is considerably less affected here than by its counterpart to the west. Within 50 km of the western end of the transform, the northern transform wall occurs 30 km north of its location over the rest of the transform.

Free-air gravity profiles recorded across the Oceanographer transform fault show values of +120 mgal over both of the transverse ridges and -60 mgal over the central valley. Schroeder (1977) reports that Bouguer corrections for these features account for practically all of the positive values over the ridges but not for all of the negative values over the central valley.

Results of work with ALVIN and ANGUS in the transform valley, presented by the Oceanographer Transform Tectonic Research Team (1980a,b), suggest that the crust in the valley itself is thin, perhaps less than 1000 m thick. The results also showed that the walls of the valley exhibit apparently dip-slip faulting, creating a stair-step effect which determines the valley-wall topography, and that the zone of active strike-slip motion is only several hundred meters wide along the center of the valley floor.

In this chapter we present an examination of the seismicity and the large earthquakes of the Oceanographer transform. We have constructed synthetic seismograms for the earthquake which occurred on 17 May 1964, the largest observed on the transform, in an attempt to determine its fault parameters and focal depth. With this and other information we have compiled about the earthquakes on the transform we have tried to answer the following questions about the transform behavior. What are

the main source parameters of this large earthquake? How deep in the crust or mantle did it occur? Was this earthquake typical of those on other transforms? What is the re-cycle time for seismic episodes on any section of the transform? Has the entire transform slipped at least once during its known seismic history?

LARGE EARTHQUAKES

The known earthquakes on the Mid-Atlantic Ridge between 34° and 36°, including the Oceanographer Fracture Zone, are listed in Table 3.1. These events were taken from Gutenberg and Richter (1954), Rothe (1969), I.S.C., and P.D.E. Reports of N.E.I.S. Figure 3.1 shows the epicenters of these events plotted on a bathymetric map of the region. The epicenters of the events which occurred prior to the establishment of WWSSN in 1963 are not as well determined as the epicenters of the more recent events.

There have been 7 events with M_S greater than or equal to 5.5 recorded from 1926 to the present whose latitudes indicate that they occurred on the Oceanographer transform. Figure 3.2 shows the longitudes of the epicenters of these events plotted versus time. (Since the transform is a linear east-west feature, longitude is a good measure of position along the transform length.) With the exception of the event in 1932, which may have been mislocated, the largest events have all occurred toward the center of the transform, as observed elsewhere by Burr and Solomon (1978) and Solomon and Burr (1979). The apparent gap in the seismicity between 1932 and 1955 is probably a reflection of the threshold of detection. Few of the events recorded since 1955 have been larger than about M_S 5.5.

THE MAY 17, 1964 EARTHQUAKE

The largest known earthquake (M_S = 6.3) on the Oceanographer Fracture Zone occurred on May 17, 1964. The fault-plane solution obtained by Sykes (1967) from P wave first motions shows left-lateral strike-slip motion on a nearly vertical fault-plane with a strike of 86°. Weidner and Aki (1973) inverted Rayleigh wave amplitude and phase spectra for this event and found a similar fault-plane solution but with a fault strike of 91°, a seismic moment of 1.94×10^{25} dyne-cm, and a focal depth of 6 ± 3 km below the sea floor. Figure 3.3 shows the fault-plane solutions obtained by both Sykes (1967) and Weidner and Aki (1973).

We have studied the May 17,1964 event by computing synthetic P wave seismograms using the method described in Chapter 2. P wave synthesis for this event can augment the surface wave study of Weidner and Aki (1973) because body waves and surface waves generally contain different information about the event. In particular the P waveforms of shallow strike-slip events vary much more rapidly with depth than do the spectra of Rayleigh waves, which show little variation for events with depths up to about 10 km. Our method of P wave synthesis also allows for a finite source rather than a point source as used in the inversion of Weidner and Aki (1973).

One disadvantage of P wave synthesis over surface wave inversion is that observed P waves have much smaller amplitudes than Rayleigh waves and the signal to noise ratio is therefore smaller, prohibitively so for events with $m_b < 5.5$. P wave synthesis, like surface wave analysis, depends on knowledge of the ground structure near the source; the near-source body-wave velocities determine the emergent angles of the P, pP, and sP waves. For vertical strike-slip events the amplitude ratios

of these three components depend solely on the emergent angles and not on station azimuths. While these ratios do not vary much within the narrow range of possible emergent angles, the overall amplitudes, and thus the scalar seismic moment of the event, vary with emergent angles. If the velocities used are too low, for example, the emerging rays will be calculated as too close to vertical, in this case the B axis, and the radiation pattern will therefore produce synthetic P waves that are too small. In compensation, the seismic moment needed to match synthetic amplitudes to observed ones will be too large. Velocities at the source also determine the delay times of the pP and sP phases after the P phase, and thus influence the final waveform and, indirectly, the focal depth inferred.

For this event we used the P waves from 20 WWSSN stations; station data are given in Table 3.2. The records were digitized over a time length large enough to include that entire portion of the P wave, generally about 60 sec. Synthetic seismograms were then constructed to provide a visual match to the observed seismograms, with particular attention given to predominant periods, slopes of rising and falling portions of the waveforms, and the existence and shape of any features in the early portion of each waveform. Features after about 10 sec into the observed waveforms were ignored because they were probably due to water reflections which we did not included in our synthesis. Three stations used, BEC, MAL, and TOL, were closer than 30° and thus may have been influenced by multiple arrivals of the P wave associated with the upper mantle transition zone. For this reason we did not give as much consideration to these stations as to the others, though only BEC, the closest of the three, was difficult to fit. The positions of the stations used on the lower focal hemisphere are shown in Figure 3.4. The

source structure used is shown in Table 3.3. This structure was obtained by seismic refraction by Detrick and Purdy (1980) for the Kane Fracture Zone east of the Kane transform fault. (Their experiment is one of the most detailed studies of crustal stucture under a fracture zone, and the Kane and Oceanographer transform faults have similar physiographic characteristics.) Results of the fits of synthetic and observed waveforms are given in Figure 3.5.

The most significant feature of the seismograms for this event is that the waveforms recorded at the stations in the western hemisphere look quite different from those recorded at stations in the eastern hemisphere. Except for station BEC, the waveforms observed to the west all had a double-peaked initial pulse, and many also had a small precursory phase ahead of the main arrival. The waveforms observed to the east all had a smooth, highly emergent initial pulse, and a predominant period of this pulse perhaps 50% longer than those observed to the west. Figure 3.6 presents some actual seismograms of this event which illustrate these features. These features must of course be reflected in the parameters used to construct synthetic seismograms, so that the source time function used for each hemisphere should be different. In our synthetic seismograms we obtain a double peak for the western hemisphere stations if the focal depth is sufficiently large that the P phase is separated from the pP and sP phases. The longer, smoother waveforms observed to the east can be produced in our synthetic seismograms if the rupture propagation is unilateral from east to west, which results in a merging of the double peaks into one. We were not able to reproduce quite the level of emergence observed in the waveforms from the eastern stations. We suggest that this may have been due to the

same precursory phase observed in the seismograms of the western stations.

We also considered an alternate set of fault parameters for these waveforms by using a multiple source, with a second source located to the east of and later than the first. We discuss this alternate source discription later in this chapter.

We found a seismic moment for this event of 9.9×10^{25} dyne-cm. This is greater than the value of 1.94×10^{25} dyne-cm found by Weidner and Aki (1973). Since the scalar moment represents a scaling factor for the synthetic seismograms, we determined the value reported here by averaging the moment determined for each station, using the formula

$$\ln M_0 = 1/n \sum_i \ln M_{0i} \qquad (3.1)$$

where n is the number of stations used and M_{0i} is the moment for station i which gave the best fit of the amplitudes of the observed and synthetic seismograms. Using this approach allows us to express the uncertainty in M_0 by determining the standard-deviation σ of $\ln M_0$; thus $\exp(\sigma)$ represents an "error factor" for M_0. The 2σ lower limit for M_0 was 2.2×10^{25} dyne-cm and the upper limit for M_0 was 4.4×10^{26} dyne-cm. One station, SHA, was considerably outside of the 2σ range, i.e., differing by a factor of 13.4 compared to the 2σ error of a factor of 4.5. This error was probably due to the proximity of the ray path to one of the nodal planes, where the amplitudes vary most rapidly with changes in the relative angle between ray and nodal plane; the amplitudes for such stations are strongly dependent on the velocity structure used, as the emergent angles vary with velocity at the source. The last column of Table 3.2 gives the values of moment found for each station. All of these values are larger than the value of M_0 found by Weidner and Aki

(1973), and their value for M_0 is slightly outside of the 2σ range presented here. Our value for this event is slightly less than the values found by Kanamori and Stewart (1976) for two events on the Gibbs transform, 3.4×10^{26} dyne-cm for an event with M_S 6.3, and 4.5×10^{26} dyne-cm for an event with M_S 6.9.

The seismic moment determined here was susceptible to other kinds of error than the statistical scatter discussed above. Of particular concern is the dependence of maximum amplitude on the phasing of the P, pP, and sP. In synthesizing a double peak for the stations to the west, we required a depth so that the pP and sP phases, which arrived close enough together compared to the signal length that they acted as one phase, to begin motion in the same direction as the initial motion of the P phase just after the P phase had begun to change direction. This destructive phasing reduced amplitudes in a way strongly dependent on the depth and signal length. Another serious source of error is the inverse proportionality of the calculated amplitudes on the cube of the seismic velocity at the source. We used the lower of the two mantle velocities presented by Detrick and Purdy (1980); had we used a still lower velocity it would have meant larger synthetic amplitudes and therefore a smaller moment. (A lower velocity also would have produced smaller emergent angles, placing the ray paths closer to the nearly vertical B axis. This would have meant smaller amplitudes but the effect would have been less than that produced directly by a lower velocity. Perhaps the Detrick and Purdy (1980) velocity structure is not representative of the Oceanographer transform fault.)

The depth we found for this event was 4.0 km below sea floor. This value is similar to that found by Weidner and Aki (1973), who placed this event at 6 km below sea floor, but admitted a range of 3 to 10 km. The value determined here is more precise because the synthetic P waveforms vary strongly with changes in depth of only a kilometer, while the surface wave radiation pattern from a strike-slip earthquake is relatively insensitive to changes in depth within the upper 10 km of a typical ocean floor structure. Figure 3.7 shows two synthetic seismograms calculated for the same station for this event, one using a focal depth of 4.0 km below sea floor and the other using a depth of 5.0 km below sea floor, with other parameters held constant. To some extent, the effect on the waveform of increasing the focal depth can be compensated by increasing the fault length and rise time so that the shape of the source time function and the ratio of its length to the delay times of the pP and sP phases is constant. While this will maintain a constant waveform shape, it will change the predominant periods of the waveform, in this case making the waveform too long. We believe that the depth presented here is precise to about ± 1 km, subject to the velocity structure used.

The fault-plane solution used to calculate the synthetic seismograms for this event is shown in Figure 3.4, along with the positions of the rays to each of the twenty stations used. The fault-plane solution shown has a fault strike of 277°, a dip of 89.5° to the north, and a slip angle of 4°, using the convention of Kanamori and Stewart (1976). The fault strike was originally chosen to be 277° because that is close to the average strike of the active part of the fracture zone. (The direction of horizontal slippage predicted by the rotation pole given by

Minster et al. (1974) is 281° but their confidence limits allow the strike to be as low as 270°.) However a change in the strike of only 5° in either direction makes it difficult to obtain simultaneous fits of the waveforms for more than just a few stations. For stations in North America better fits of the waveforms could generally be obtained by decreasing the dip, thus moving the east-west striking nodal plane closer to the emergent directions of the rays to these stations. The limiting factors to this are the waveforms and amplitudes observed at SHA and ATL, for which compressional first-arrivals must be maintained, and for which the amplitudes of the synthetic seismograms become too small if the dip is decreased too much. The synthetic seismograms calculated for both of these stations show the effects of this compromise. The fit of the waveform for BEC could be improved by moving the east-west striking nodal plane the other direction, so that it dips to the south. However this would cause a deterioration in the fits for most of the North American stations. (We suspect that the poor fit obtained for BEC may be due to the proximity of the station to the epicenter.) We have given the dip to a precision of 0.5°, because that was necessary to obtain a satisfactory fit at SHA and ATL. However since emergent angles depend on the poorly known velocity structure, the actual uncertainty on the dip of the fault plane is probably closer to ± 5°, even though the relative angle between rays and fault plane is more constrained. The slip angle can be varied about 3° in either direction from that given without significant variation in the synthetic waveforms, other than a change in the relative amplitudes for stations to the east compared with those to the west.

If we assume completely unilateral propagation, we can determine fault length because the difference between eastern and western time

functions is proportional to the fault length. The fault length used for the synthetic seismograms was 12 km. This value has an uncertainty of about ± 2 km, given the model of unilateral propagation. It is possible that there was a bilateral component even though the propagation was primarily unilateral. If so the actual fault length may have been somewhat larger, though not larger by an amount that contributed substantially to the waveform. The width was set at 5 km because a larger value, say, 10 km as used by Kanamori and Stewart (1976), produced source time functions which were too long. This value for width is compatible with the depth determined (4 km below sea floor) in that we would expect rupture to extend at least from the point of origin upward to include the top of the igneous crust and probably downward also. The effect of this fault width is to add approximately 1 sec to the length of the source time function for all stations, since the fault plane is nearly vertical. The effect of minor variations in the fault width could easily be absorbed by variations in the rise time or propagation velocity, and thus width is not well-constrained.

The rise time used was 1 sec. Propagation was taken to be horizontal and unilateral, east to west, in order to reproduce the difference between the observed seismograms from the eastern and western hemispheres. The rupture propagation velocity used was 4 km/sec rather than the more commonly used value of 3 km/ sec. With a fault length of 12 km, a rupture velocity of 3 km/sec would have lengthened all of the source time functions by 1 sec, thus requiring either a shorter fault length incompatible with the observed difference between waveforms to the east and the west, or a much shorter (i.e., zero) rise time, or a zero fault width, or some combination of these effects. Though we obtained our fits

with the value of 4 km/sec, we do not claim to have determined rupture propagation velocity, and we recognize that this value is greater than the shear wave velocity in the crust. The overall length of the source time functions necessary to match the observed seismograms was about 3 to 3.5 sec to the west and about 4.5 to 5 sec to the east; an increase in either the rise time or fault dimensions, or a decrease in the propagation velocity, would have made the source time functions unacceptably long unless there were some compensating effect, such as the previously mentioned possibility of a bilateral component to the rupture propagation.

The observed difference in the waveforms from east to west could not be explained by a difference in attenuation using bilateral propagation. Increasing the value of t^* for stations to the east lengthens the waveforms but not nearly enough to match the observed waveforms. In addition, an increase in t^* smooths out the details in the region of maximum displacement of the first motion so that the synthetic waveforms are not nearly as "peaky" as the observed ones. With the values used for these synthetic seismograms we were able to match not only the "peakiness" and predominant period but also the general asymmetry in the maximum amplitude portion of the first motion in all of the observed seismograms from stations in the eastern hemisphere.

Using the above values for scalar moment and fault dimensions, and using a value for shear modulus μ of 3.5×10^{11} dyne/cm^2, we calculate that the average displacement for this event was about 5 m. Dividing this by the rise time of 1 sec produces a dislocation velocity of 5 m/sec. This value is close to the range of previously reported dislocation velocities (Brune, 1970; Kanamori, 1972; Abe, 1974), and does

not agree with the exceptionally low dislocation velocities (0.1 to 0.2 m/sec) determined by Kanamori and Stewart (1976) for two large events on the Gibbs Fracture Zone. Our value of dislocation velocity is determined to no better than ± 50% however because of low precision in the value for rise time, which could be varied between 0.5 and 1.5 sec without significant change in the synthetic seismograms. Since the values of displacement and dislocation velocity were determined from the values for fault dimensions and total moment, which have their own uncertainties, we have confidence only in the order of magnitude determined for dislocation velocity.

An additional source of imprecision is the quasi-ambiguity in the effect of rise time and fault width on the calculated source time functions: both effects involve a convolution of the source time function with a rectangular "boxcar" function. The effects are not strictly ambiguous; however for horizontal propagation on a vertical fault the only way in which these effects are seen differently at different stations is a dependence of the fault-width effect on emergent angle, an effect which is particularly weak over the narrow range of epicentral distances for these stations. The quasi-ambiguity between these values is such that their effects on dislocation velocity are somewhat offsetting, though not entirely so, because their effects on the source time functions do not trade off in perfect inverse proportionality.

We have determined the stress drop for this earthquake using the formula given by Kanamori and Anderson (1975) for a strike slip event

$$\Delta\sigma = \frac{2}{\pi} \mu \frac{D}{W} \qquad (3.2)$$

where μ is shear modulus of the material, D is the average displacement, and w is the fault width. For (3.2) we adopted values of μ and fault width as used for the synthetic seismograms and the calculated displacement value presented earlier. We obtained a value of stress drop of about 200 bars, which is high compared to the range of stress drops presented by Kanamori and Anderson (1975) for inter-plate events. Since stress drop is proportional to seismic moment, if our moment value is too large, as suggested by the discrepency between our value and that of Weidner and Aki (1973), the stress drop value should be lower. Likewise, a greater fault length would have meant a smaller displacement, and therefore a lower stress drop. Had we used a fault width smaller by, say, a factor of 2, and accepting our moment value, it would have meant a displacement larger by the same factor, and thus an extremely high stress drop of approximately 800 bars; had we used a width of 10 km it would have meant a stress drop of only 50 bars.

As mentioned earlier, we were able to generate waveforms similar to those observed by using a very different set of source parameters. For this exercise we placed the focal depth right at sea floor, so that the P, pP, and sP phases were not separated in time. We then modeled the double peak observed in the western hemisphere by using a multiple source, with a second source located to the east of and later than the first. By adjusting the spatial and temporal separations we were able to create two peaks to the west by having the arrivals separated while the two signals arrived simultaneously to the east. We prepared synthetic seismograms for two stations, STU to the east, and OGD to the west. The results are shown in Figure 3.8. For these we used bilateral faulting on faults which were each 7 km long, a rupture propagation velocity of 3

km/sec, fault strikes = 95°, dips = 90°, slip angles = 0°, fault widths = 5 km, and rise times of 0.5 sec. The second source was located 7 km east of the first, on an azimuth of N95°E relative to the first, and 2.5 sec later. The moments used were 4.0×10^{25} dyne-cm for the first source and 8.0×10^{25} dyne-cm for the second. The synthetic waveforms do not fit those observed as well as do those prepared from a single source, in that the synthetic waveform is too long for OGD and too short for STU. It was difficult to correct both of these problems simultaneously. For this reason and because the two additional parameters create too many degrees of freedom to allow any real precision in the results, we did not try to generate synthetic seismograms for other stations. We present this case to illustrate that the observed waveforms could be explained (although not necessarily equally well) by at least two source models. In the single source model, the propagation is continuous from east to west, while in the double source model, propagation is discrete, from west to east. The two models required similar total moments however, 9.9×10^{25} dyne-cm for the single source model, and 1.2×10^{26} dyne-cm for the double source model.

The suggestion of high stress drop and unilateral propagation on a 12 km fault is noteworthy considering the teleseismic location of the event, which placed it just north of an irregularity in the bathymetry about 15 to 20 km east of the western end of the transform; see Figure 3.1. (The epicenter may have been mislocated to the north because of a large number of seismic stations whose azimuths were to the north.) This bathymetric feature may be related to a local stress concentration or asperity on the transform. The three previous large earthquakes on the Oceanographer Fracture Zone, in 1957, 1959, and 1960, were located either near the

epicenter of the 1964 event or further to the east, and thus may have released the strain on those sections of the fault. Our interpretation is that the 1964 event initiated at a stress concentration or fault asperity related to the local bathymetry and propagated westward toward the junction of the fault and the adjoining ridge segment.

THE NOVEMBER 18,1970 EARTHQUAKE

Figure 3.9 shows the fault plane solution, constructed from both P-wave polarities and S-wave polarization angles, for the event which occurred on the Oceanographer Fracture Zone on November 18, 1970 (m_b = 5.1). This fault plane solution is quite similar to that of the 1964 event; in fact, the arrivals in Figure 3.9 can be accomodated very well by the same fault plane solution as that found for the 1964 event. The 1970 event also displayed some form of precursory or multiple event activity. Figure 3.10 shows the short-period vertical seismogram for station DUG (epicentral distance 59.3°, azimuth 300°). The arrival time marked A was that reported by I.S.C. This station's arrival time had a residual of -5.1 sec, almost exactly the time difference between the arrival marked A and that marked B in Figure 3.10. This suggests that the epicenter and origin time determined by I.S.C. for this event probably corresponded to this second arrival, implying that many stations must have reported the second arrival and not the first. A histogram of the residuals reported by I.S.C. for their teleseismically-located epicenter is shown in Figure 3.11. Such a large scatter would result if there were actually two (or more) nearly simultaneous events separated by perhaps 50 km and if the two events were interpreted as one for the epicentral location. If such a hypothesis were correct for this event, multiple events may not be uncommon for large earthquakes on the

Oceanographer transform. We have not tried to study this event further because it was too small for the precision necessary to resolve any useful information about its source parameters.

TOTAL ACCUMULATED MOMENT

Because the transform is a plate boundary, we would expect that potential seismic moment is continouously generated by the relative motion between the plates. We can therefore compare the total moment from observed earthquakes to the slip rate estimated from magnetic anomalies.

For all of the earthquakes on the Oceanographer transform listed in Table 3.1 we have estimated the seismic moment from M_S using the formula

$$\log M_0 = 19.1 + 1.04\ M_S. \qquad (3.3)$$

We obtained this formula by fitting a straight line to the transform fault data presented by Burr and Solomon (1978), using the M_0 value of 9.9×10^{25} dyne-cm for the 5/17/64 earthquake. Using Weidner and Aki's (1973) value for this event made very little difference in the formula. The moments so calculated are given in Table 3.4. Summing the moments from all of the known earthquakes over this time period, as described by Brune (1968), gives a value for observed seismic moment of 2.3×10^{26} dyne-cm. Note that the 1964 earthquake contributes half of this value.

To this we added a correction to account for events with M_0 smaller than those observed. This correction is calculated from formula (7) given in Molnar (1979)

$$\dot{M}_0^{\Sigma} = \frac{\alpha}{1 - \beta}\ M_0^{max(1-\beta)} \qquad (3.4)$$

where $\dot{M}_0^{\Sigma}$ is the total rate of moment generation, M_0^{max} is the maximum moment to be included in the summation, and α and β are defined as

$$\alpha = 10^{(a+bd/c)} \qquad \text{and } \beta = b/c.$$

The quantities a and b are empirically determined values from the equation

$$\log N(M) = a - b\,M \tag{3.5}$$

where N(M) is the number of events with $M_S \geq M$, and c and d are from the empirically determined equation

$$\log M_0 = c\,M_S + d. \tag{3.6}$$

We used c = 1.04 and d = 19.1 as presented above. We found values for a and b by fitting a straight line to the distribution of events given in Table 3.1, using only those events which were definitely on the Oceanographer transform, and normalizing the values of N(M) to a one year period. For the period 1964 to 1981, we used events from M_S 4.5 to 6.3. This excludes the very smallest event, the M_S 4.3 earthquake on 12/12/67; Table 3.1 can not be counted on as being complete for events of this size. We obtained values of a = 3.47 and b = 0.773. For the value of $M_0^{max} = 3.5 \times 10^{23}$ dyne-cm (the smallest observed between 1964 and 1981) we obtain a value of 1.9×10^{24} dyne-cm/yr as the rate of moment accumulation for events up to this size. Multiplying this by 18 years gives a moment accumulation of 3.4×10^{25} dyne-cm for these smaller (undetected) events. Similar calculations for the years between 1920 (the apparent time when the Gutenberg and Richter (1954) listings became sensitive to events as small as M_S = 5.6) and 1964, with the same values of a and b and with the smallest observed M_0 of 7.8×10^{24} dyne-cm, gives a moment accumulation rate of 4.2×10^{24} dyne-cm/yr and a total moment

accumulation of 1.8×10^{26} dyne-cm for the undetected events during these years.

Adding these corrections to the total observed seismic moment of 2.3×10^{26} dyne-cm for the time from 1920 to the present gives us a total seismic moment of 4.5×10^{26} dyne-cm.

From the transform dimensions and slip rate we have calculated the total moment which would have accumulated on the transform fault from 1920 to the present, using

$$M_0 = \mu L w D \tag{3.7}$$

where μ is the shear modulus, L is fault length, w is fault width, and D is total displacement over the 61 year span. For this calculation we used $\mu = 3.5 \times 10^{11}$ dyne/cm^2, L = 130 km, w = 5 km, and D = 145 cm, calculated using the rotation poles and rotation rates determined by Minster et al. (1974). We used a width of 5 km because that value was assumed for the 17 May 1964 event. The result was an expected total seismic moment of 3.7×10^{26} dyne-cm.

The moment sum calculated from the seismicity is thus approximately equal to that expected from the slip rate and transform dimensions. This result suggests that most of the slippage on the transform occurs as earthquake activity. However Brune (1968) stated that the potential error in the moment of each event may be as great as a factor of 5, and we have made the additional conversion of m_b to M_S for most of the events since 1964. Therefore the near equality between expected and observed total moments should not be judged as particularly significant.

A major source of uncertainty in this equality is the value of the expected moment calculated from slip rate using (3.7). The value of μ we

used may not be accurate for transform material. The least well known quantity in (3.7) is the fault width. If the seismic thickness for the whole transform is not uniform, and the average is therefore different from 5 km by some factor, then our expected moment sum would have been different by that factor, and the agreement with the observed value would have been poorer.

SEISMICITY

Several of the earthquake epicenters displayed in Figure 3.1 are considerably to the west of the western end of the active transform section. We believe that these events were mislocated. Events of this size and frequency represent a source of significant displacement, and would most certainly be accompanied by smaller events, yet ocean-bottom seismometer surveys of the microearthquake seismicity at ridge-transform intersections, including the eastern end of the Oceanographer transform (e.g., Rowlett, 1981), show very little or no seismicity on the inactive side of ridge-transform intersections. The epicenters of the remaining events shown in Figure 3.1 as well removed from the Oceanographer transform suggest that they occurred on the smaller transform segments which lie just to the north and south of the Oceanographer transform, and that the sections of the Mid-Atlantic Ridge adjacent to the Oceanographer transform have been seismically quiet.

The teleseismically determined epicenters are scattered over the transform in a zone perhaps 30 km wide. This may be because a lack of a significant number of stations to the north or south prevents any precision in the determination of latitude, or it may be real, indicating that seismic activity is not confined to a narrow zone of slippage.

If, as suggested by ALVIN and ANGUS studies, the zone of active strike-slip motion is limited to the transform valley center, then possibly the observed minor seismicity is made up primarily of dip-slip events which build the valley walls, and thus may indeed be scattered over the entire valley width. Verifying this would require the observation of enough P-wave first arrival polarities from some of these smaller events to distinguish between these two kinds of orientations; the same smallness which makes these events difficult to locate precisely also makes reliable first motion polarities difficult to obtain.

The locations of seismic activity may also be related to the topography. The first of the two events on August 16, 1965, for example, was located teleseismically to be on that part of the northern wall which was discussed earlier as bending northward to form a pocket. This location may indicate that this event is in some way related to whatever process produced this topographic feature.

The fault length we found for the May 17,1964 event, the largest on the transform since the deployment of WWSSN and possibly the largest ever recorded, was only 12 km, considerably smaller than the transform length of 130 km. Such limitations on event size are also common on other transforms, e.g., the Romanche transform fault. This discrepency between potential fault length and actual fault length may indicate that the crust or lithosphere is broken by a number of distinct fault segments and that an episode of transform slip occurs along an isolated segment rather than the entire transform.

CONCLUSIONS

From the observations presented in this chapter we can draw some inferences in general about the seismic processes occurring on the Oceanographer transform fault, and in particular about the largest event observed on the transform. The 1964 earthquake was definitely strike-slip, with a vertical fault plane whose strike was parallel to the topographically-inferred direction of the transform. The rupture propagation of this earthquake was primarily, if not completely, unilateral, with the predominant direction from east to west, though west to east propagation is also possible if the event were composed of two (or more) discrete sources. The depth of this earthquake was 4 ± 1 km below the sea floor if the source was a single event, placing the focus in or near mantle material; a greater focal depth can be excluded while a shallower depth, e.g., at the sea floor, is possible if the rupture were of the discrete west-to-east type mentioned above. Stress drop, displacement, and dislocation velocity for this event do not appear to have been abnormal for events of this size. Comparison of this event to the events on the Gibbs transform fault studied by Kanamori and Stewart (1976) shows this one to be more "normal"; the events on the Gibbs transform required source time functions with total lengths of 17 and 22 sec, implying low stress drops and low dislocation velocities. A source time function this long is incompatible with the P waveforms observed for this event, for which the source time functions were in the range of 4 to 5 sec.

One implication of the 1964 event is that the Oceanographer transform fault slips in a jerky manner. This event had a displacement of about 5 m, while the displacement calculated from the slip rate for

the last 61 years is only about 1.6 m. While there is significant imprecision in the displacement calculated for the 1964 event, the actual displacement for this event was probably much larger than that expected from the slip rate. These figures suggest that the repeat time for an earthquake similar to the 1964 event on this part of the transform is about 200 years, and a recurrence time for large events ($M_S \geq 6.0$) on the whole transform is about 15 to 20 years. This last result is supported by the seismicity listed in Table 3.1, which shows 4 events with $M_S \geq 6$ since 1920. The short (12 km) fault length for the 1964 event is considerably less than the transform length, which allows for a large number of events to take place before this section of the transform fractures again. In all, the transform has not slipped uniformly in the last 61 years. While there has been fairly steady backgound seismicity, there have been only a few events large enough to release a significant amount of strain, of which the 1964 event was probably the largest. If a fault length of about 12 km is representative of the earthquakes on the Oceanographer transform with $M_S \geq 6.0$, then there have only been enough of these events to fracture less than half of the transform length since 1920.

The unilateral propagation and the location of the 1964 earthquake suggest that there may be a relation between bathymetric features and the seismicity and fault parameters of large transform earthquakes. One interpretation is that the bend in the transform trend near the western end causes a stress concentration, which helps generate large earthquakes there. The larger events are also seen to be concentrated around the central portion of the transform, which is likely to be cooler and therefore also more likely to sustain larger earthquakes.

Finally it appears that multiple, or at least non-simple, seismic sources may be fairly common on this transform. One conjectural explanation of precursors such as that seen for the 17 May 1964 earthquake is that they represent the breaking of weaker material, an event which concentrates stress in an adjacent stonger (cooler or locked) section of the fault, causing that section to break in a larger earthquake with perhaps a higher stress drop.

Table 3.1. Earthquakes on or near the Oceanographer transform fault

Date	Origin Time h	m	s	Lat, °N	Lon, °W	h, km	m_b	M_s	No. of sta.
7/3/26	18	09	53	35.5	36	-		(d)	-
12/4/32	4	04	00	35.5	36.5	-		6	-
5/6/55	11	39	58	35.3	36.8	-		(d)	-
2/10/57(n)	5	47	59	35.5	34.6			5.8	-
12/23/57	12	34	08	35.2	35.8	-		6	-
3/19/59	8	25	32	35.1	36.1	-		6.2	-
6/8/60	16	19	48	35.0	35.0	-		5.9	-
5/17/64	19	26	21.6	35.35	36.08	33	5.6	6.3	210
8/16/65	4	36	37.1	35.4	35.75	16	4.6	(4.7)	71
8/16/65	19	53	18.3	35.2	35.1	52±85	4.7	(4.9)	49
8/17/65	0	22	25.5	35.0	35.0	33	4.4	(4.5)	28
7/15/66	2	26	15.4	35.4	36.35	33	4.6	(4.7)	24
12/12/67	11	50	08	35.0	35.3	33	4.3	(4.3)	10
5/2/68(n)	7	33	50	35.8	35.3	-	4.0	(3.9)	4
7/21/69	17	38	29.8	35.35	36.05	33	4.9	4.8	101
8/4/69	13	47	00.0	35.60	36.58	33	4.7	(4.9)	20
11/5/70(s)	20	36	14	34.78	37.09	54±55	5.0	(5.3)	45
11/18/70	12	23	15.6	35.14	35.90	18±2	5.1	(5.4)	218
7/2/71	3	35	49.2	35.32	36.39	33	4.7	(4.9)	82
6/17/72	6	00	4.4	35.27	35.45	0	-	-	10
7/5/72	4	06	13.0	35.47	36.61	26±1	4.4	(4.5)	36
11/26/72	8	00	42.1	35.40	36.46	25±30	5.0	(5.3)	71
5/8/73(n)	0	26	11.9	35.78	34.62	33	4.0	(3.9)	13
2/2/74(n)	3	37	26	35.65	34.51	41±23	4.9	(5.2)	77
3/6/74	5	11	04.1	35.00	35.24	33	4.4	(4.5)	15
3/10/74	20	14	42.6	35.3	31.5	33	4.5	(4.6)	12
4/17/74	0	32	21.4	35.2	35.37	28±3	5.0	5.0	136
9/9/74(s)	17	58	10	34.6	36.63	56±32	5.0	4.5	42
5/24/75(s)	2	37	38.9	34.4	36.84	33	4.6	(4.7)	12
3/26/76(n)	11	08	09	35.5	34.2	33	4.7	(4.9)	27
1/16/77	10	34	54.2	35.44	37.07	10	4.9	(5.2)	56
3/28/77(s)	13	00	16	34.69	36.75	28±34	4.8	(5.0)	41

Table 3.1 continued

4/29/80	16 02 45.6	35.32	36.33	10	5.1	4.7	88
7/14/80	4 24 24.4	35.14	35.45	10	5.2	5.1	105
1/9/81	7 51 28.3	35.18	35.21	10	4.9	5.0	33

Data for the events of 1926 and 1932 were taken from Gutenberg and Richter (1954). Data for events between 1955 and 1964 inclusive were taken from Rothe (1969). Data for events from 1964 to 1977 were taken from the ISC Regional Bulletin, while events in 1980 and 1981 were taken from P.D.E. reports of the U.S.G.S. M_S values for events before 1964 are the values reported with the other data; d refers to a Gutenberg and Richter (1954) listing as between 5.3 and 5.9, assumed here to be 5.6. M_S values shown in parentheses for events after 1964 were determined from m_b and the formula $M_S = 1.36\ m_b - 1.49$, obtained as a least squares fit to the data for oceanic transform earthquakes of Burr and Solomon (1978) plus the 5 events listed in this table definitely on the Oceanographer transform fault for which both M_S and m_b values were available. The notation (n) or (s) after the date of an event denotes a probable location on the small transforms to the north and south, respectively, of the Oceanographer transform.

Table 3.2. Station data used for synthetic seismograms for the earthquake of May 17, 1964

Station	Distance, degrees	Azimuth, degrees	Magnification	M_o, 10^{25} dyne-cm
BEC	23.9	271.1	1500	5.1
MAL	25.6	77.6	750	10
TOL	25.7	70.3	1500	7.3
ESK	30.1	38.2	1500	6.5
OGD	30.6	292.4	3000	10
SCP	33.1	292.2	750	11
STU	35.7	53.7	750	5.6
AAM	37.3	295.4	1500	11
CAR	37.4	236.2	3000	5.4
KON	38.2	36.0	1500	3.6
TRI	38.7	59.0	3000	6.1
ATL	39.6	281.6	1500	23
FLO	42.9	291.3	1500	13
SHA	43.5	279.2	1500	130
MNN	43.9	300.6	3000	6.9
RCD	51.1	301.4	750	21
ALQ	56.4	291.7	3000	7.7
BOZ	56.4	305.3	3000	7.7
TUC	60.7	290.5	1500	14
BKS	66.7	300.7	3000	8.3

For all stations we used T_p = 30 sec, T_g = 100 sec, H_p = .93, H_g = 1.0, where T_p, T_g, H_p, and H_g refer to the seismometer and galvanometer periods and damping factors, respectively.

Table 3.3. Source structure used for synthetic seismograms for event on May 17, 1964

	Layer	Thickness, km	V_p, km/sec	ρ, g/cm^3
1.	water	4	--	--
2.	crust	2.4	4.7	2.8
3.	mantle	Half-space	7.8	3.3

Table 3.4 Moment values for earthquakes on the Oceanographer transform fault

Date	M_o, 10^{24} dyne-cm
7/3/26	7.8
12/4/32	20.
5/6/55	7.8
12/23/57	20.
3/19/59	33.
6/8/60	16.
5/17/64	99.
8/16/65	0.91
8/16/65	1.5
8/17/65	0.56
7/15/66	0.91
12/12/67	0.35
7/21/69	1.2
8/4/69	1.5
11/18/70	4.8
7/2/71	1.5
7/5/72	0.56
11/26/72	3.8
3/6/74	0.56
3/10/74	0.71
4/17/74	1.9
1/16/77	3.0
4/29/80	0.91
7/14/80	2.4
1/9/81	1.9

Values for all events except 17 May 1964 were calculated using the M_S values reported in Table 3.1 and the equation $\log M_0 = 1.04 M_S + 19.1$ obtained from the data of Burr and Solomon (1978), excluding the M_S 7.9 event of 10 November 1942 and using the value determined here of 9.9×10^{25} dyne-cm for the event of 17 May 1964.

Figure Captions

Figure 3.1 Bathymetry of the Oceanographer Fracture Zone in the vicinity of the Mid-Atlantic Ridge, and epicenters of all known earthquakes in this area. The approximate location of the ridge axis is indicated by double lines. The squares represent epicenters taken from Gutenberg and Richter (1954) and Rothe (1969). Larger symbols are those events with $M_S > 6.0$. Contour intevals are every 1000 m below sea level, taken from Rogan, M., 1982.

Figure 3.2 Longitude versus year of occurrence for the 7 earthquakes on the Oceanographer transform fault with $M_S > 5.5$. Symbols are the same as for Figure 3.1.

Figure 3.3 Fault plane solutions for the May 17, 1964, Oceanographer transform earthquake, obtained by Sykes (1967) (solid line) and Weidner and Aki (1973) (dashed line).

Figure 3.4 Positions on lower focal hemisphere of stations used for synthesis of P waves for the May 17, 1964 earthquake, and fault plane solution obtained (solid line). For comparison, the fault plane solution obtained by Weidner and Aki (1973) is also shown (dashed line).

Figure 3.5 (a to e) Results of fits of synthetic (upper) and observed (lower) seismograms of P waves from May 17, 1964 earthquake. Line segments above the synthetic seismogram for each station represent the relative size and arrival times of the P, pP, and sP phases. The apparent delay between the line segments and the synthetic seismogram arrivals is caused by the attenuation operator.

Figure 3.6 (a,b) Long-period vertical seismograms of P waves from the May 17, 1964 earthquake from stations MAL and MNN. P waves show an emergent waveform at stations to the east and a double-peaked wave form at stations to the west.

Figure 3.7 Synthetic P-wave seismograms for the May 17, 1964 earthquake, calculated for station OGD using focal depths of 8 km (the preferred depth) and 9 km below sea level (4 and 5 km below sea floor), keeping other parameters constant.

Figure 3.8 Synthetic seismograms for the May 17, 1964 earthquake, calculated for stations STU and OGD using a double source. Fault parameters are described in the text.

Figure 3.9 Fault plane solution for the earthquake of November 18, 1970 on the Oceanographer transform fault, obtained from P wave first motions and S wave polarities. Open circles represent dilational arrivals; closed circles represent compressional arrivals. Smaller symbols represent questionable readings. Arrows represent the direction of S wave polarization. Arrows pointing inward represent downward SV motion; arrows pointing outward represent upward SV motion.

Figure 3.10 Short-period vertical seismogram from station DUG for the earthquake on November 18, 1980 on the Oceanographer transform fault. Arrival marked A is that reported by I.S.C. Arrival marked B, approximately 5 sec later, is from the phase probably located by I.S.C. for this earthquake. The residual determined by I.S.C. for this station was -5.1 sec.

Figure 3.11 Histogram of P-wave residuals reported by I.S.C. for the earthquake of Novembr 18, 1970 on the Oceanographer transform fault.

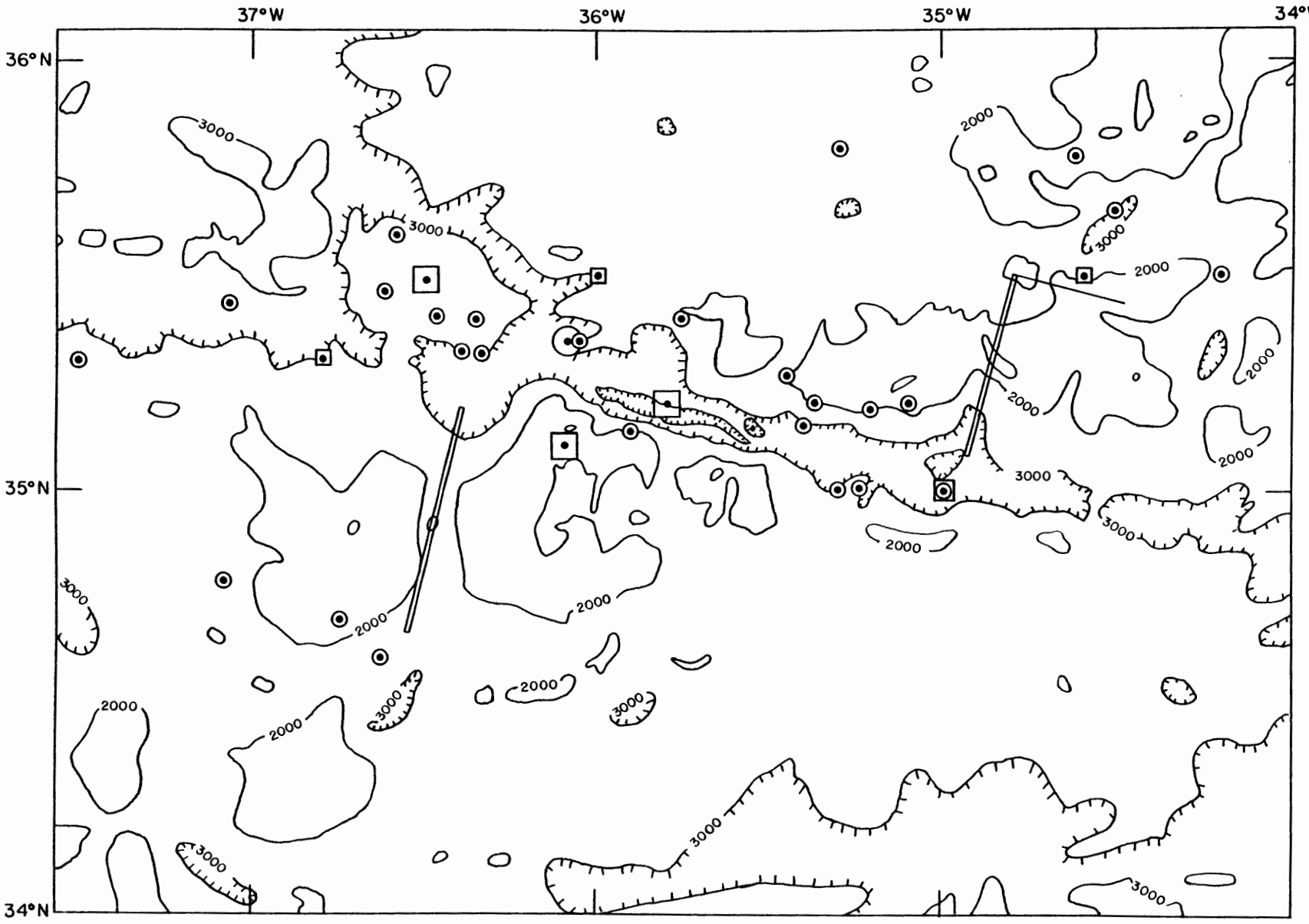

Figure 3.1

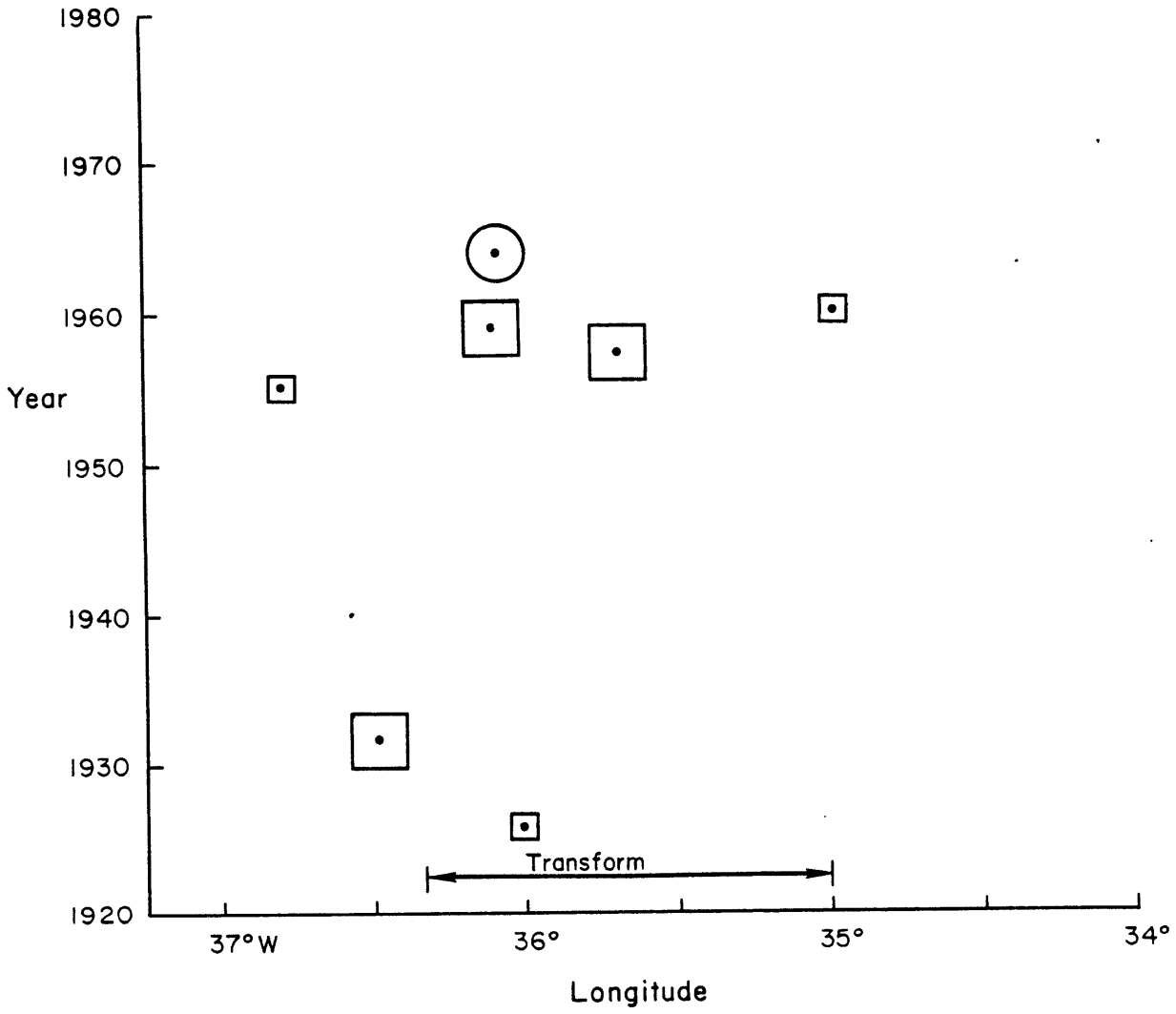
1980
1970
1960
1950
1940
1930
1920
Year
Transform
37°W
36°
35°
34°
Longitude

Figure 3.2

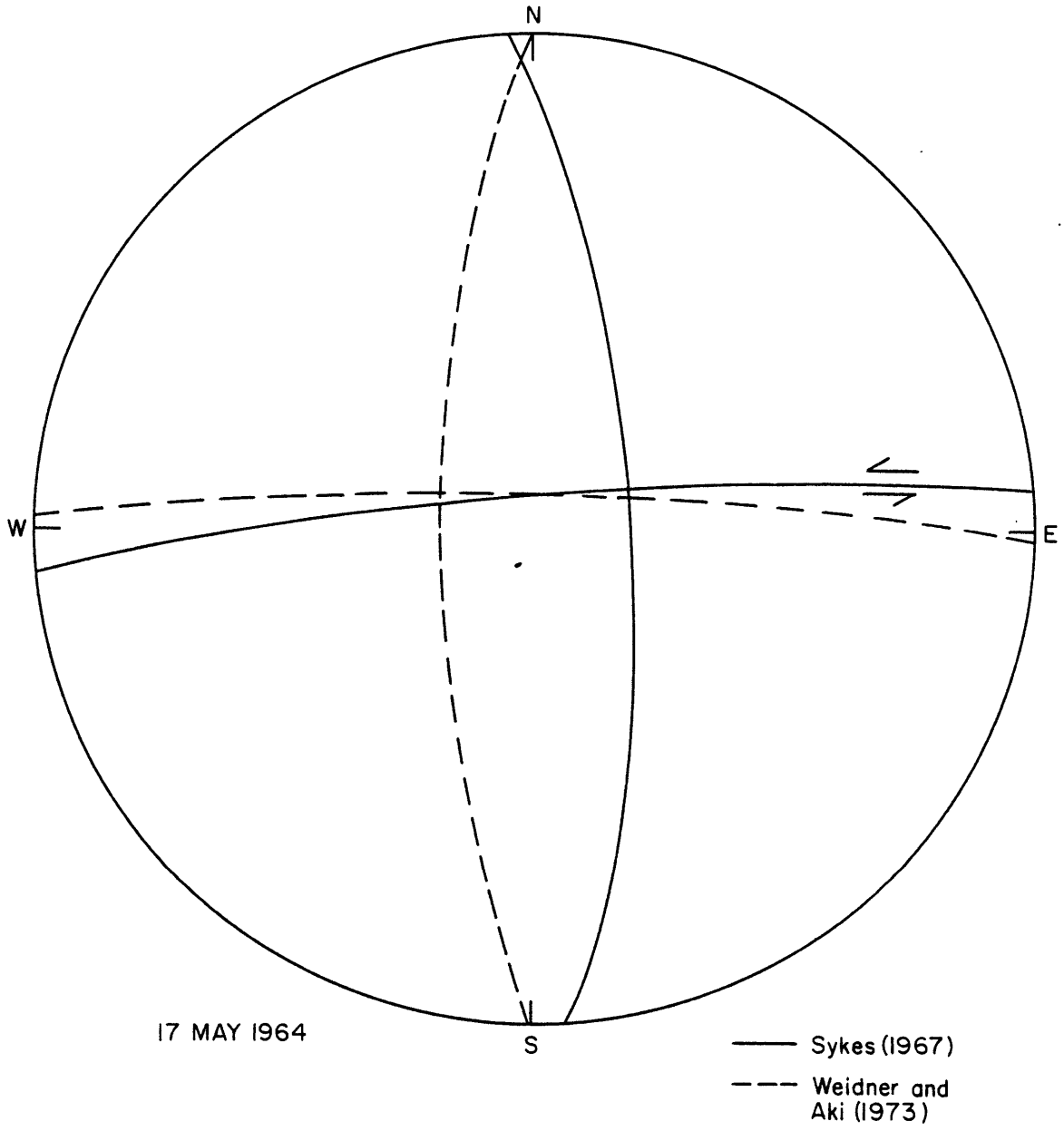

Figure 3.3

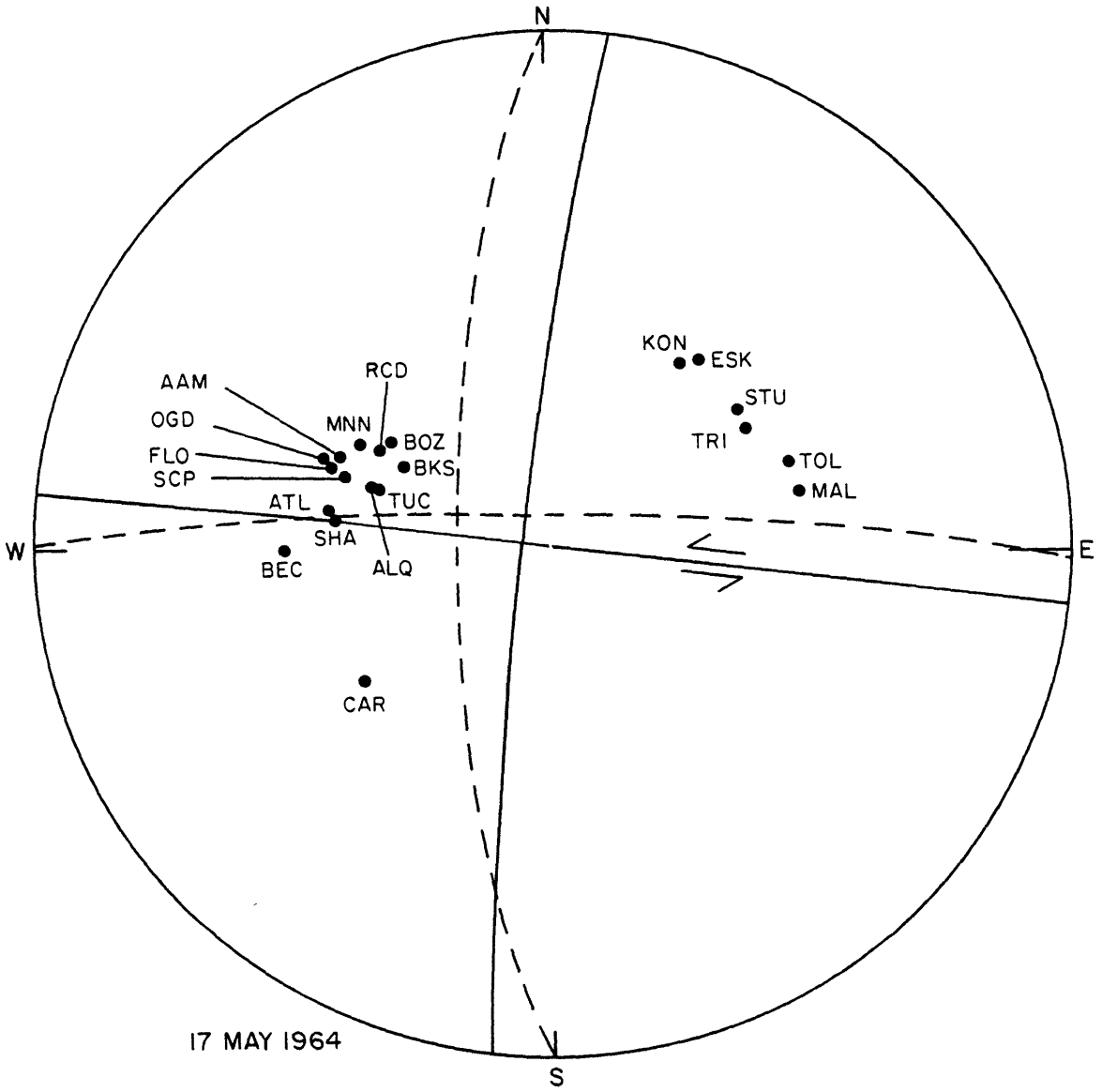
N
W
E
S
AAM
OGD
FLO
SCP
RCD
MNN
BOZ
BKS
ATL
TUC
SHA
BEC
ALQ
CAR
KON
ESK
STU
TRI
TOL
MAL
17 MAY 1964

Figure 3.4

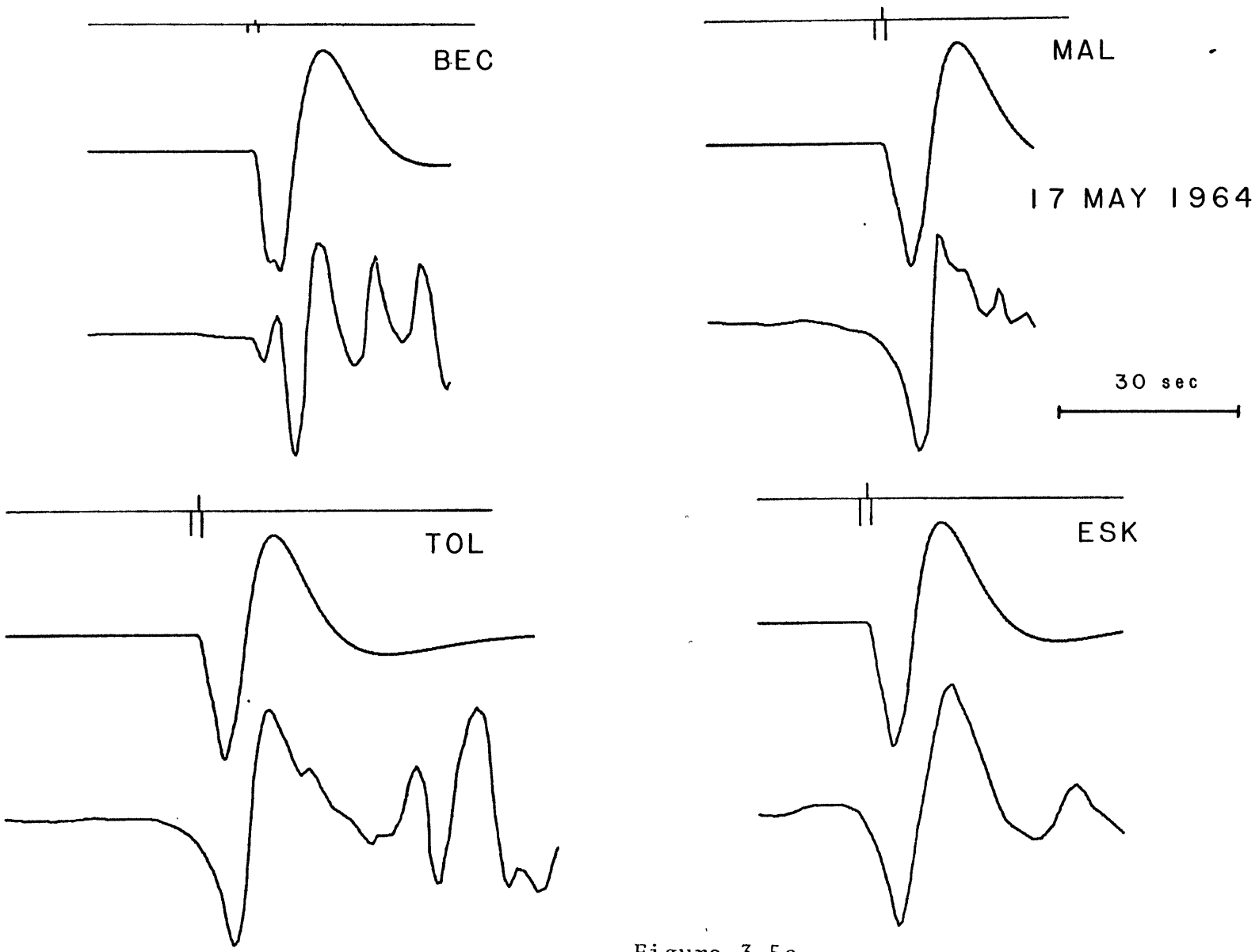

Figure 3.5a

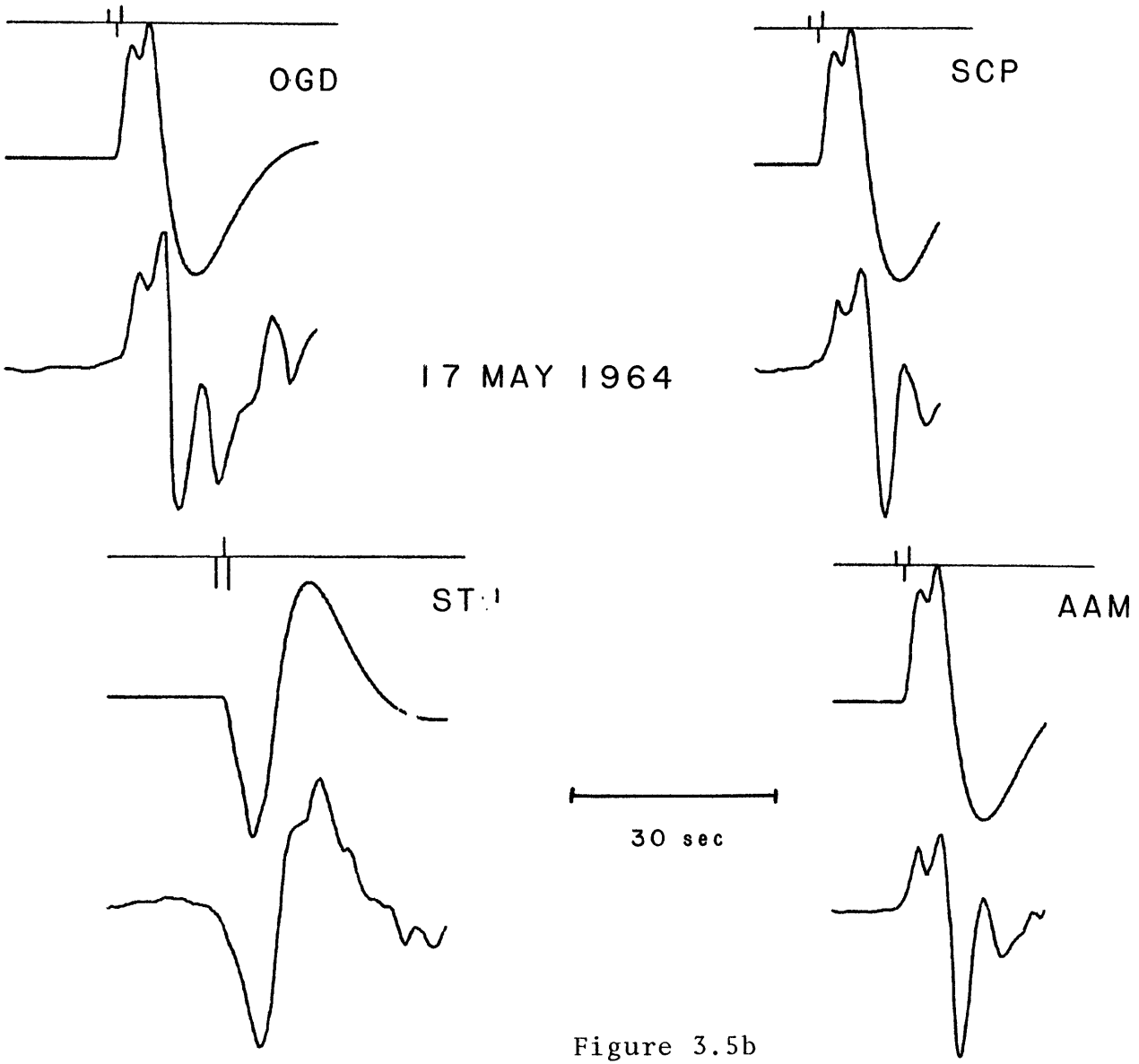

Figure 3.5b

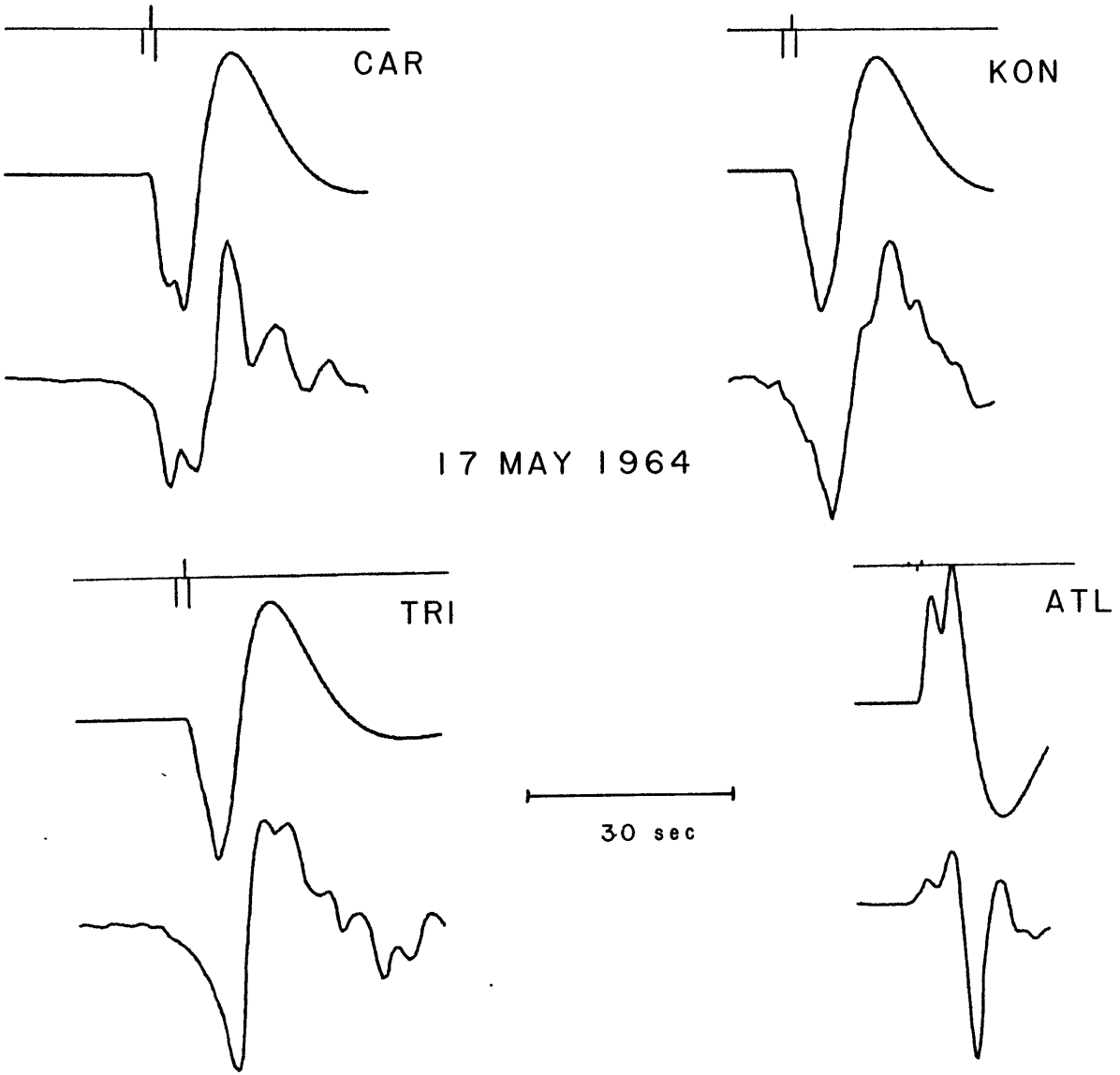

Figure 3.5c

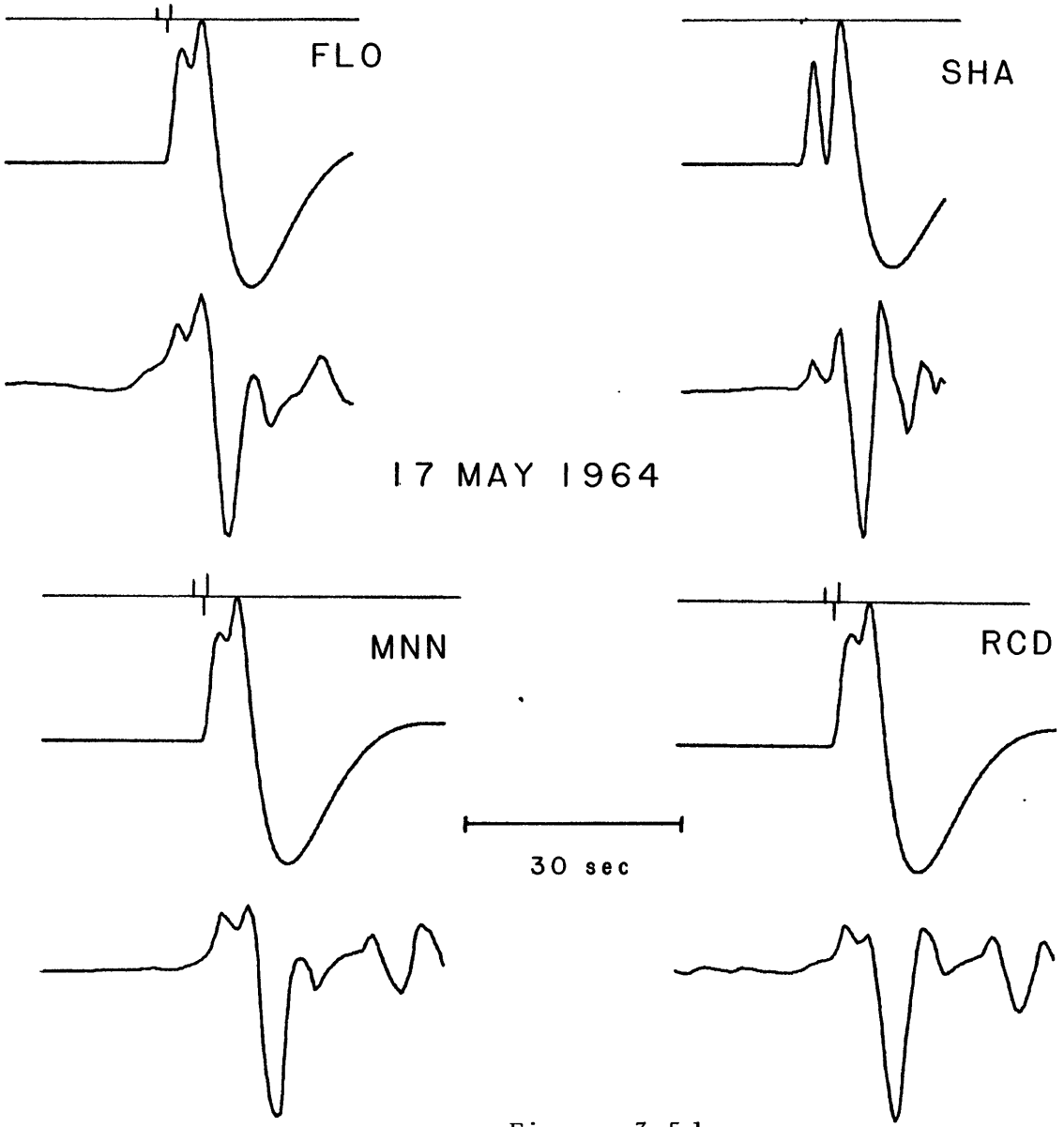

Figure 3.5d

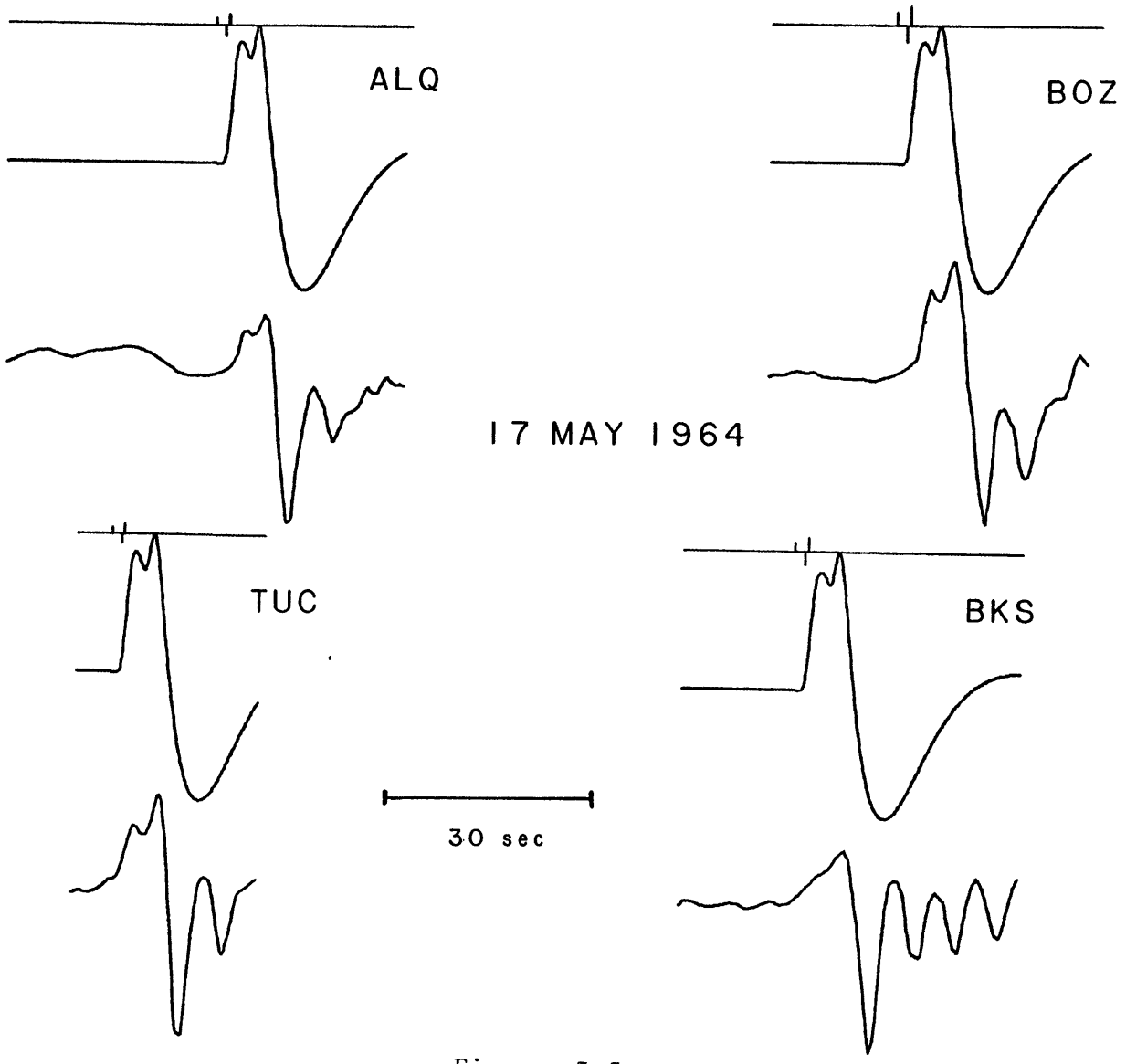

Figure 3.5e

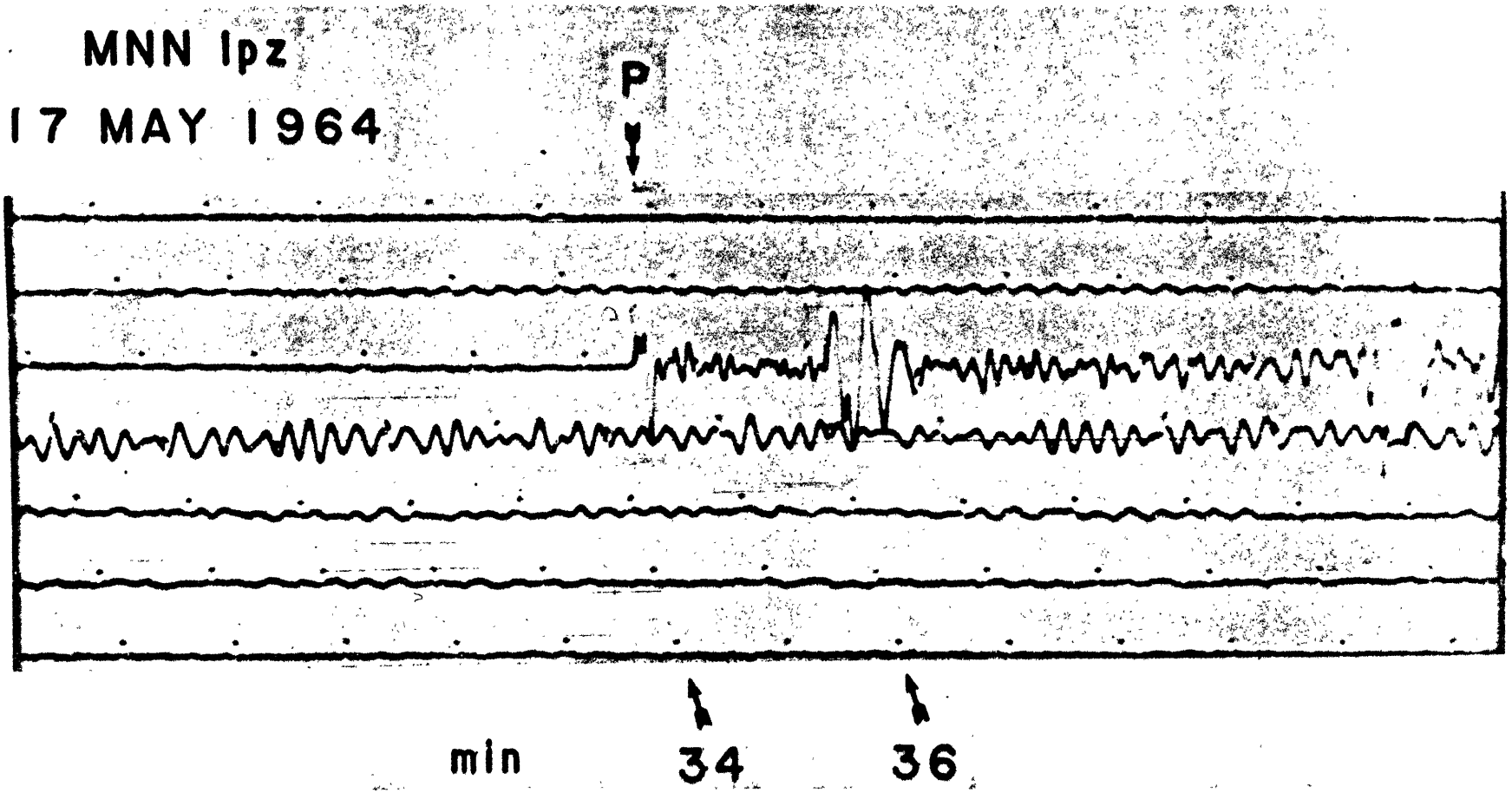

Figure 3.6a

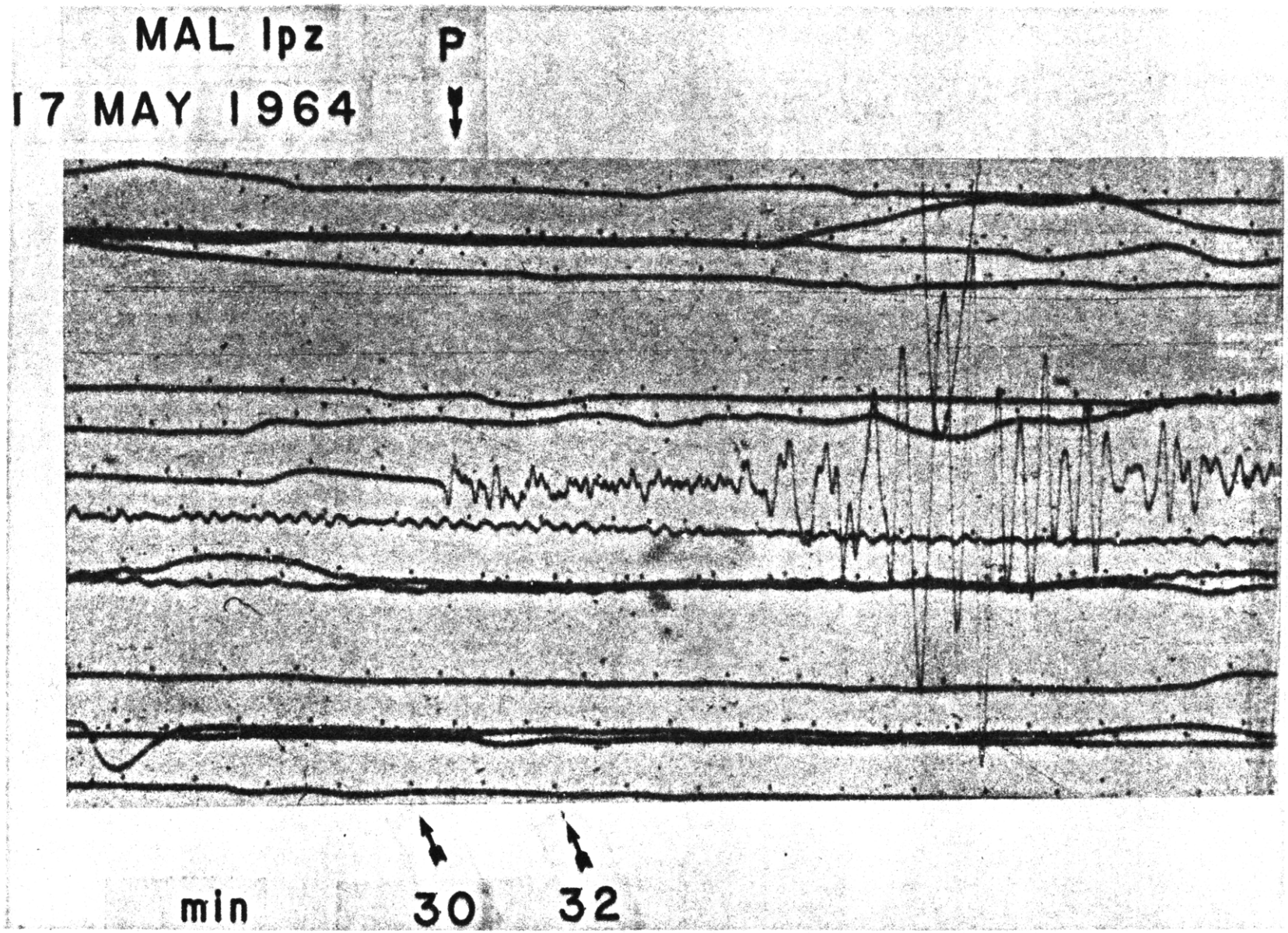

Figure 3.6b

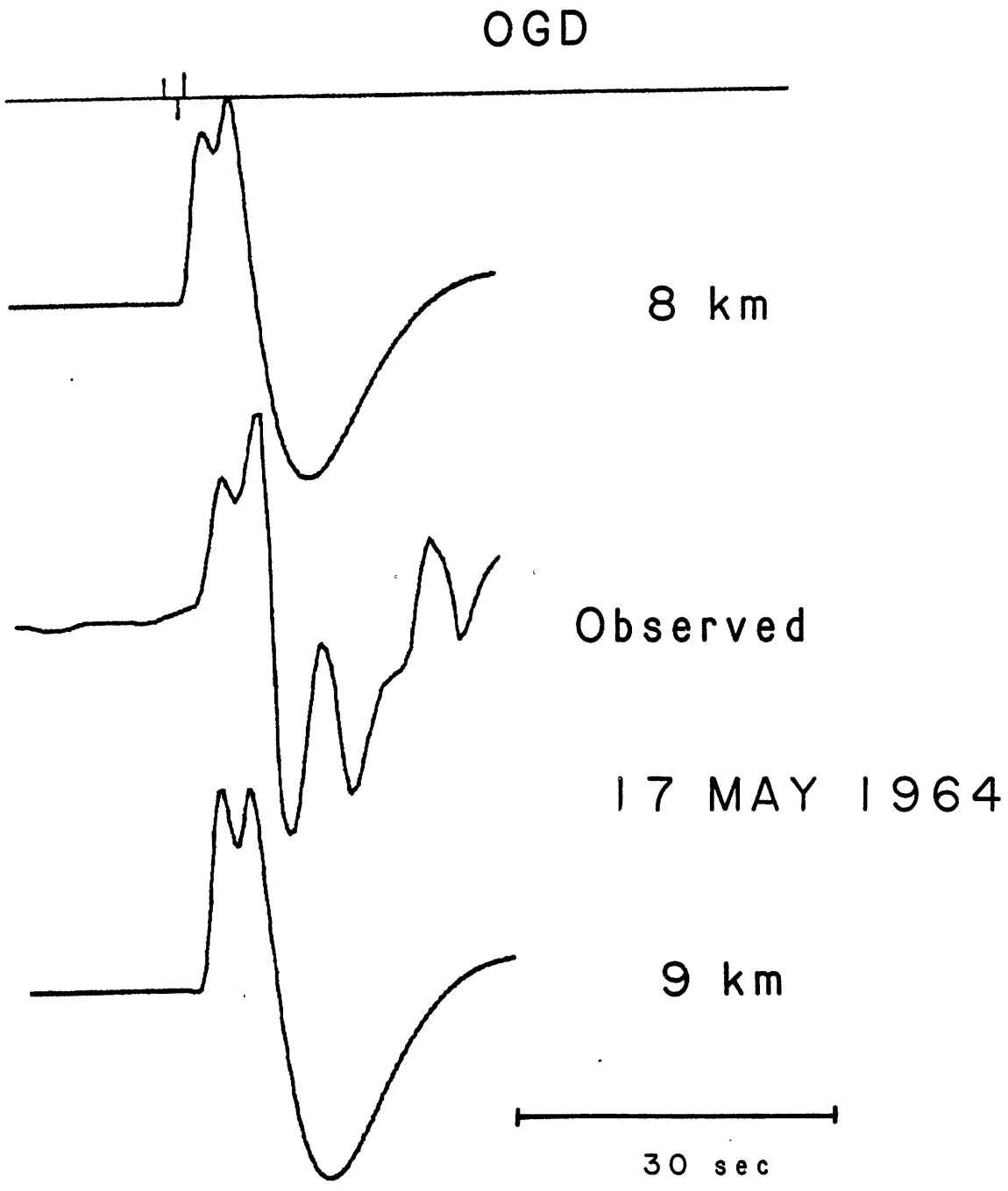

Figure 3.7

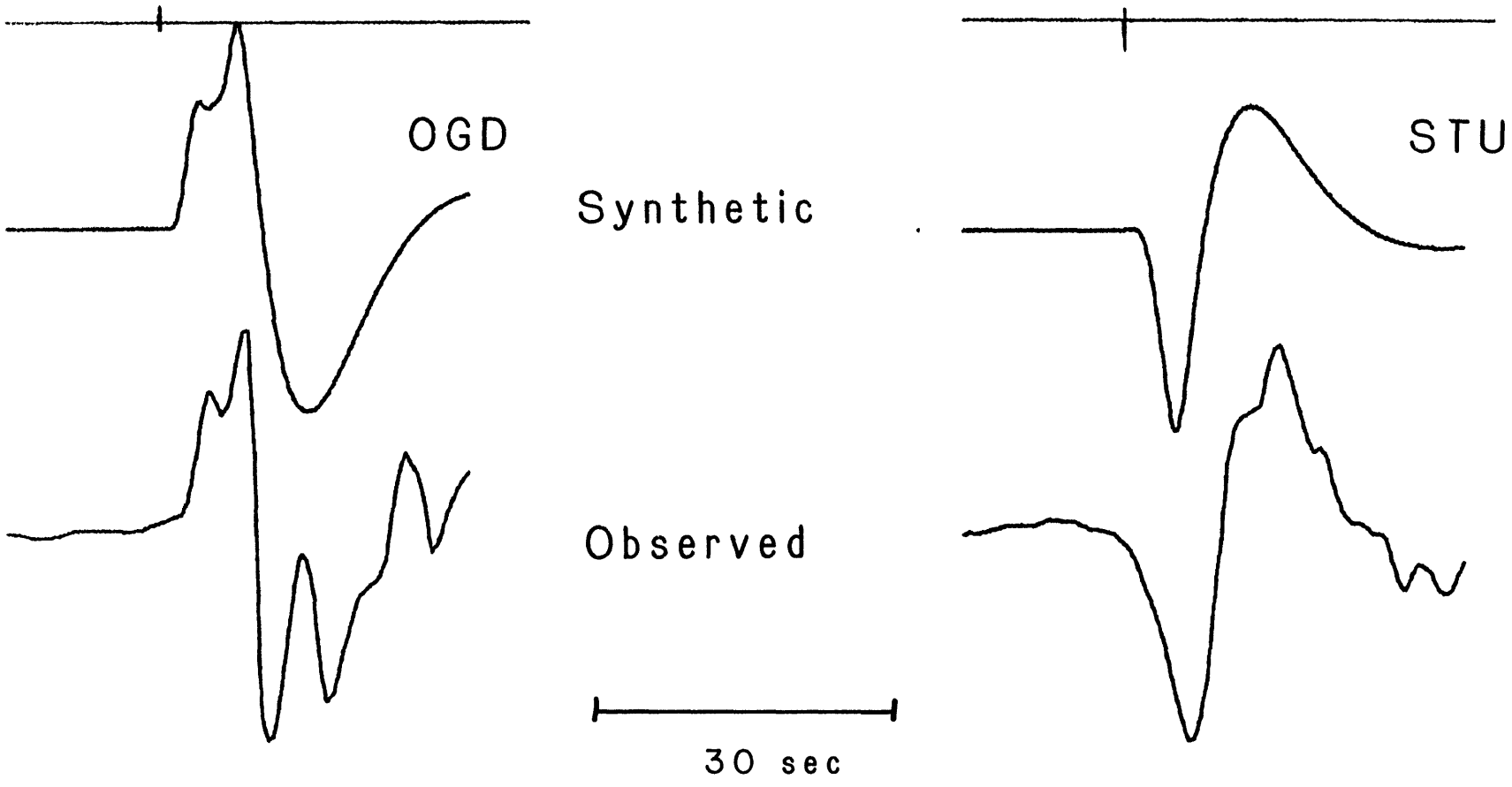
OGD
Synthetic
STU
Observed
30 sec
17 MAY 1964
Multiple Source

Figure 3.8

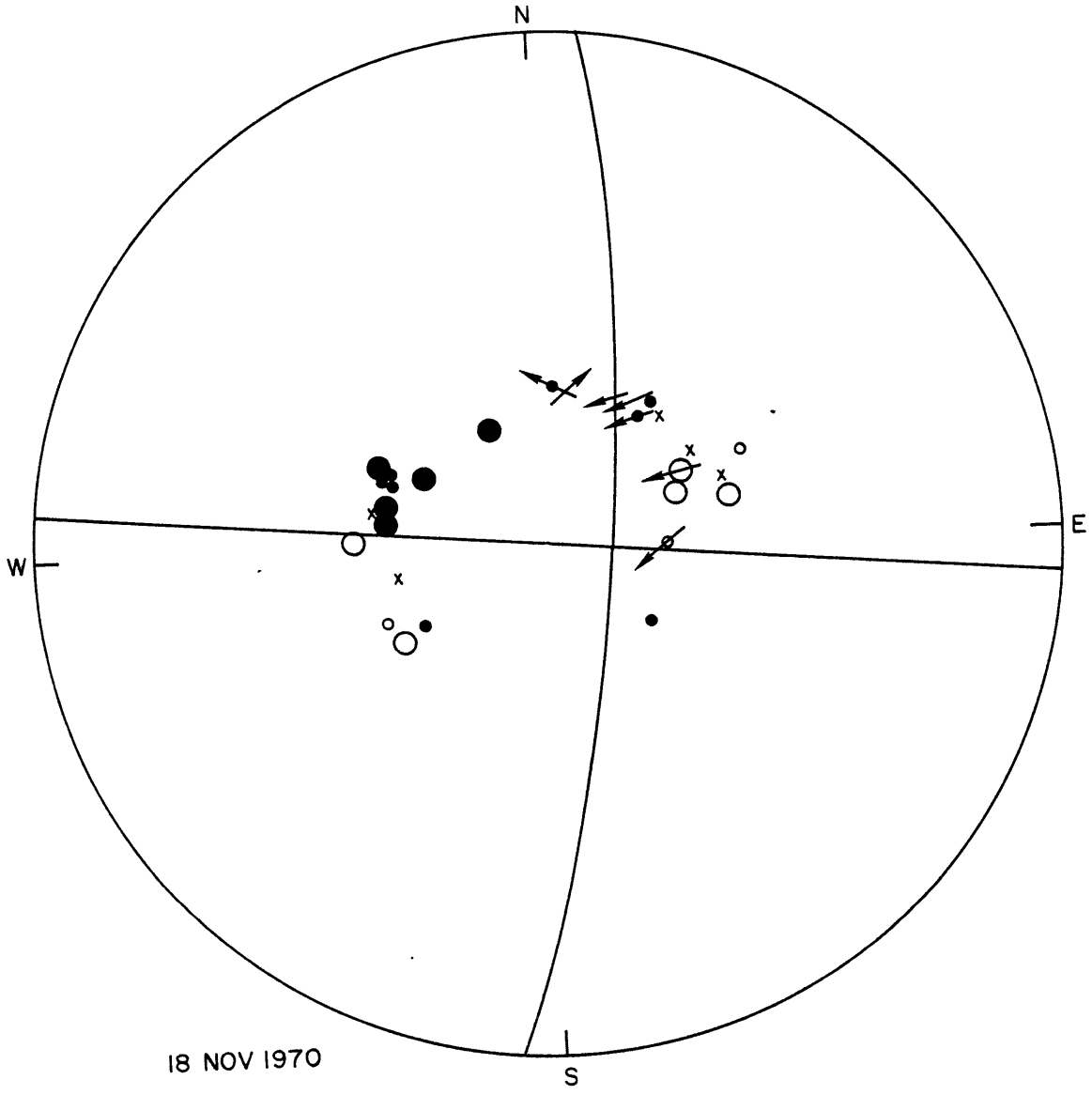

Figure 3.9

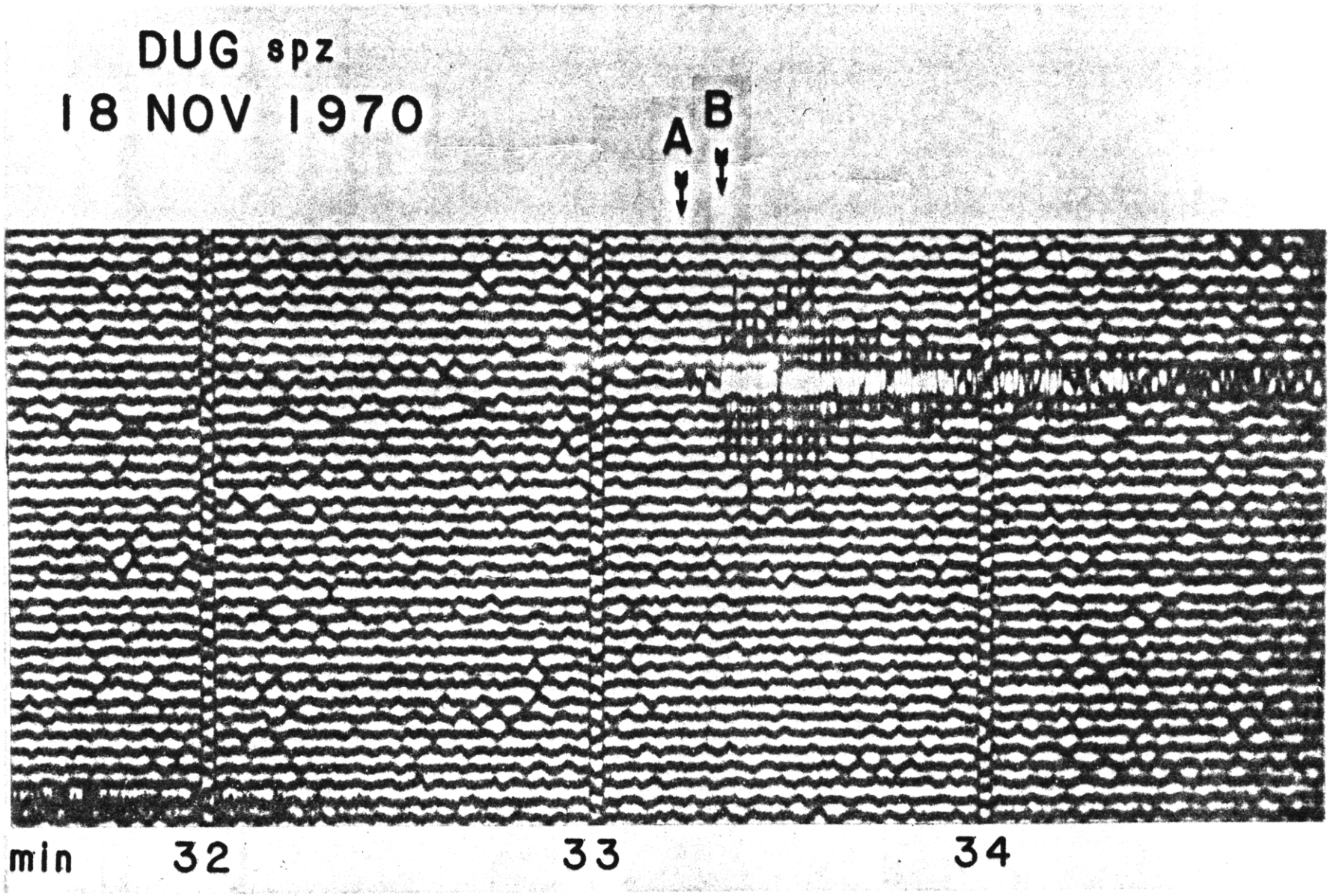

Figure 3.10

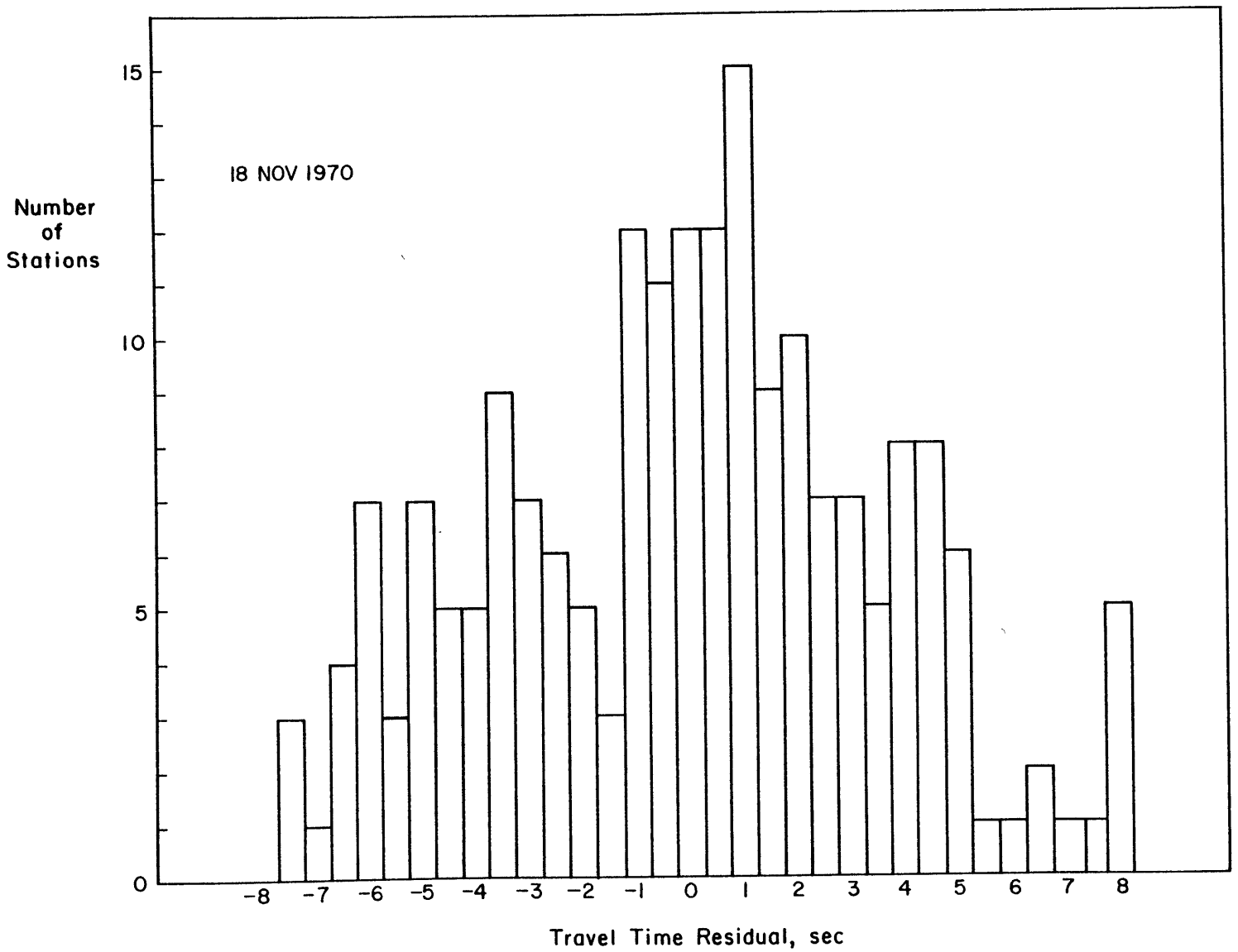
18 NOV 1970
Number of Stations
0
5
10
15
-8
-7
-6
-5
-4
-3
-2
-1
0
1
2
3
4
5
6
7
8
Travel Time Residual, sec

Figure 3.11

CHAPTER 4. PLANS AND OBJECTIVES FOR FUTURE WORK

The work presented here is a study of large earthquakes on the Oceanographer transform fault. The results presented show that the source parameters of a large earthquake and the type of motion on this transform are different from that found by Kanamori and Stewart (1976) for the Gibbs transform. The obvious question to ask is which of these two transforms, if either, represents more normal behavoir? Both of these transform faults may be unusual, as indicated by the results of Kanamori and Stewart (1976) for the Gibbs transform, and by the infrequency of large earthquakes for the Oceanographer transform. More generally, can the earthquake tectonics of transforms be described by any uniform characterization? Since transforms exhibit a wide range of lengths and slip rates, and since some features of transform seismicity have been shown to be related to these transform characteristics, we might expect large differences in the behavior of different transforms. To answer these questions we must look at other transform faults.

In addition to these issues, there are a number of questions which this study has failed to answer. We have not been able to explain the observed differences between the Oceanographer and Gibbs transforms. We have not resolved whether the background seismicity represents fault motion of a different type from that associated with the larger events. We have not resolved the possibly related issue of whether the seismic zones are actually as wide as they appear to be from teleseismically-determined epicenters.

To address these questions we intend to extend the study presented here to other transform faults in the North Atlantic. We are particularly interested in the the Vema transform, the 15° 20' N

transform, the Kane transform, the Hayes transform, and the Atlantis transform.

Our additional work on large earthquakes will include inversion of Rayleigh wave amplitudes and phases to determine the source moment tensor. [We did not do this for the earthquake of May 17, 1964 because Weidner and Aki (1973) had already modeled the surface waves.] Moment tensor inversion will provide an additional check on focal depths, fault plane solutions, and seismic moments. We will also relocate the epicenters of some smaller transform earthquakes, using the master-event relocation method of Chung and Kanamori (1976). [This method requires a good azimuthal distribution of stations for which arrivals have been observed at both the master event and the event being relocated. We did not have good distributions available for any event pairs on the Oceanographer transform.]

REFERENCES

Abe, K., Fault parameters determined by near- and far-field data: the Wakasa Bay earthquakes of March 26, 1963, Bull. Seis. Soc. Am., 64, 1369-1382, 1974.

Abe, K. and H. Kanamori, Magnitudes of great shallow earthquakes from 1953-1977, Tectonophysics, 62, 191-203, 1980.

ARCYANA, Transform fault and rift valley from bathyscaph and diving saucer, Science, 190, 108-116, 1975.

Bouchon, M. and K. Aki, Discrete wave-number representation of seismic source wave fields, Bull. Seis. Soc. Am., 67, 259-277, 1977.

Brune, J. N., Seismic moment, seismicity, and rate of slip along major fault zones, J. Geophys. Res., 73, 777-784, 1968.

Brune, J. N., Tectonic stress and the spectra of seismic shear waves from earthquakes, J. Geophys. Res., 75, 4997-5009, 1970.

Bullen, K. E., An Introduction to the Theory of Seismology, Cambridge University Press, Cambridge, 3rd ed., 381 pp., 1965.

Burr, N. C. and S. C. Solomon, The relationship of source parameters of oceanic transform earthquakes to plate velocity and transform length, J. Geophys Res., 83, 1193-1205, 1978.

Carpenter, E. W., Absorption of elastic waves- an operator for a constant Q mechanism, AWRE Report O-43/66, Her Majesty's Stationery Office, London, 1966.

Chung, W.-Y. and H. Kanamori, Source process and tectonic implications of the Spanish deep-focus earthquake of March 29, 1954, Phys. Earth Planet. Int., 13, 85-96, 1976.

Detrick, R., J. Mudie, B. Luyendyk, and K. Macdonald, Near-bottom observation of an active transform fault: Mid-Atlantic Ridge at 37° N, Nature, 246, 59-61,1973.

Detrick, R. S., Jr., and G. M. Purdy, The crustal structure of the Kane Fracture Zone from seismic refraction studies, J. Geophys. Res., 85, 3759-3777, 1980.

Eittreim, S. and J. Ewing, Vema Fracture Zone transform fault, Geology, 3, 555-558, 1975.

Ewing, W. M., W. S. Jardetzky, and F. Press, Elastic Waves in Layered Media, McGraw-Hill, New York, 380 pp., 1957.

Fleming, H. S., N. Z. Cherkis, and J. R. Heirtzler, The Gibbs Fracture Zone: a double fracture zone at 52° 30' N in the Atlantic Ocean, Mar. Geophys. Res., 1, 37-45, 1970.

Fox, P. J., A. Lowrie, and B. C. Heezen, Oceanographer Fracture Zone, Deep-Sea Research, 16, 59-66, 1069.

Fox, P. J., E. Schreiber, H. Rowlett, and K. McCamy, The geology of the Oceanographer Fracture Zone - a model for fracture zones, J. Geophys. Res., 81, 4117-4128, 1976.

Futterman, W. I., Dispersive body waves, J. Geophys. Res., 67, 5279-5291, 1962.

Gutenberg, B. and C. F. Richter, Seismicity of the Earth, 2nd ed., Princeton University Press, Princeton, N. J., 1954.

Hagiwara, T., A note on the theory of the electromagnetic seismograph, Bull. Earthq. Res. Inst., 36, 139-164, 1958.

Heezen, B. C., M. Tharp, and M. Ewing, The floors of the oceans, 1, The North Atlantic Geol. Soc. Am. Spec. Paper 65, 122, 1959.

Herrin, E., Introduction to '1968 seismological tables for P phases', Bull. Seis. Soc. Am., 58, 1193, 1241, 1968.

Isacks, B., J. Oliver, and L. R. Sykes, Seismology and the new global tectonics, J. Geophys Res., 73, 5855-5899, 1968.

Kanamori, H., Determination of effective tectonic stress associated with earthquake faulting, the Tottori earthquake of 1943, Phys. Earth Planet. Int., 5, 426-434, 1972.

Kanamori, H., The energy release in great earthquakes, J. Geophys. Res., 82, 2981-2987, 1977.

Kanamori, H., and D. L. Anderson, Theoretical basis of some empirical relations in seismology, Bull. Seis. Soc. Am., 65, 1073-1096, 1975.

Kanamori, H., and G. S. Stewart, Mode of the strain release along the Gibbs fracture zone, mid-Atlantic ridge, Phys. Earth Planet. Int., 11, 312-332, 1976.

Kolsky, H., The propagation of stress pulses in viscoelastic solids, Phil. Mag., (8) 1, 693-710, 1956.

Langston, C. A. and D. V. Helmberger, a procedure for modelling shallow dislocation sources, Geophys. J. Roy. Astron. Soc., 42, 117-130, 1975.

Love, A. E. H., A Treatise on the Mathematical Theory of Elasticity, Cambridge, Cambridge University Press, 4th ed., 643 pp., 1934.

Ludwig, W. J. and P. D. Rabinowitz, Structure of Vema Fracture Zone, Mar. Geol., 35, 99-110, 1980.

Minster, J. B., T. H. Jordan, P. Molnar and E. Haines, Numerical modelling of instantaneous plate tectonics, Geophys. J. Roy. Astron. Soc., 36, 541-576, 1974.

Molnar, P., Earthquake recurrence intervals and plate tectonics, Bull. Seis. Soc. Am., 69, 115-133, 1979.

Oceanographer Transform Tectonic Research Team, The geology of the Oceanographer transform: submersible and deep-towed camera investigations (abstract), EOS Trans. AGU, 61, T45, 1105, 1980.

Oceanographer Transform Tectonic Research Team, The Oceanographer transform: morphotectonic character of a ridge-transform intersection (abstract), EOS Trans. AGU, 61, T44, 1105, 1980.

Project ROSE Scientists, Microearthquake activity on the Orozco Fracture Zone: Preliminary results from project ROSE, J. Geophys. Res., 86, 3783-3790, 1981.

Rogan, M., Map of Ocean Margin Drilling Area VIII-I, 1982.

Rothe, J. P., The Seismicity of the Earth, UNESCO, Paris, 336 pp., 1969.

Rowlett, H., Seismicity at intersections of spreading centers and transform faults, J. Geophys. Res., 86, 3815-3820, 1981.

Rowlett, H., and D. Forsyth, Teleseismic P-wave delay times in a major oceanic fracture zone, Geophys. Res. Lett., 6, 273-276, 1979.

Schroeder, R. W., A geophysical investigation of the oceanographer fracture zone and the mid-Atlantic ridge in the vicinity of 35 degrees north, Ph.D. Thesis, Columbia Univ., 458 pp., 1977.

Sleep, N. H. and S. Biehler, Topography and tectonics at the intersections of fracture zones with centrl rifts, J. Geophys. Res., 75, 2748-2752, 1970.

Solomon, S. C., Shear wave attenuation and melting beneath the Mid-Atlantic Ridge, J. Geophys. Res., 78, 6044-6059, 1973.

Solomon, S. C., and N. C. Burr, The relationship of source parameters of ridge-crest and transform earthquakes to the thermal structure of oceanic lithosphere, Tectonophysics, 55, 107-126, 1979.

Sykes, L. R., Mechanism of earthquakes and nature of faulting on mid-ocean ridges, J. Geophys. Res., 72, 2131-2153, 1967.

Sykes, L. R., Focal mechanism solutions for earthquakes along the world rift system, Bull. Seis. Soc. Am., 60, 1749-1752, 1970.

Toksoz, M. N., and D. H. Johnston, eds., Seismic Wave Attenuation, Soc. Explor. Geophys., Tulsa, Okla., 459 pp., 1981.

van Andel, T. H., R. P. Herzen, and J. D. Phillips, The Vema Fracture Zone and the tectonics of transverse shear zones in oceanic crustal plates, Mar. Geophys. Res., 1, 261-283, 1971.

Weidner, D. J., and K. Aki, Focal depth and mechanism of mid-ocean ridge earthquakes, J. Geophys. Res., 78, 1818-1831, 1973.

Wilson, J. T., A new class of faults and their bearing on continental drift, Nature, 207, 343-347, 1965.